Early life intestinal inflammation alters gut microbiome, impairing gut-brain communication and reproductive behavior in mice

Olivia Sullivan[1,2], Claire Sie[3], Katharine M. Ng[3], Sophie Cotton[3], Cal Rosete[2], Jordan E. Hamden[2,4], Ajay Paul Singh[5], Kristen Lee[2,4], Jennifer Kim[1,2], Huaxu Yu[6], Charlotte A. Clayton[3], Natalia A. Carranza Garcia[3], Kateryna Voznyuk[2], Jatin Choudhary[2], Nadine Plett[2], Sana Arora[2], Hans Ghezzi[7], Tao Huan[6], Kiran K. Soma[1,2,8], John-Paul J. Yu[5], Carolina Tropini[3,9,10]*, Annie Vogel Ciernia[1,2,4]*

[1]Graduate Program in Neuroscience, University of British Columbia, Vancouver, Canada

[2]Djavad Mowafaghian Centre for Brain Health, University of British Columbia, Vancouver, Canada

[3]Department of Microbiology & Immunology, University of British Columbia, Vancouver, Canada

[4]Department of Biochemistry and Molecular Biology, University of British Columbia, Vancouver, Canada

[5]Department of Radiology, University of Wisconsin School of Medicine and Public Health, Madison, Wisconsin, USA.

[6]Department of Chemistry, University of British Columbia, Vancouver, Canada

[7]Department of Bioinformatics, University of British Columbia, Vancouver, Canada

[8]Department of Psychology, University of British Columbia, Vancouver Canada

[9]School of Biomedical Engineering, University of British Columbia, Vancouver, Canada

[10]Humans and the Microbiome Program, Canadian Institute for Advanced Research (CIFAR), Toronto, Canada

*Corresponding Authors:

Carolina Tropini

Life Sciences Centre, Rm 3557

2350 Health Sciences Mall

Vancouver, British Columbia V6T 1Z3

carolina.tropini@ubc.ca

Annie Vogel Ciernia

Centre for Brain Health

2215 Wesbrook Mall

Vancouver, BC V6T2A1

annie.ciernia@ubc.ca

CRediT authorship contribution statement:

OS: Methodology, Formal Analysis, Investigation, Data Curation, Writing - Original Draft, Writing - Review & Editing, Visualization

CS: Formal Analysis, Investigation, Writing - Original Draft, Writing - Review & Editing, Visualization

KN: Methodology, Formal Analysis, Investigation, Data Curation

SC: Investigation, Data Curation, Writing - Review & Editing

CR: Methodology, Formal Analysis, Investigation, Data Curation, Writing - Original Draft, Writing - Review & Editing

JEH: Investigation, Formal Analysis, Writing - Original Draft, Writing - Review & Editing

APS: Investigation, Formal Analysis

KL: Methodology, Investigation

JK: Methodology, Formal Analysis, Investigation, Writing – Review & Editing

HY: Investigation, Formal Analysis

CAC: Investigation, Data Curation

NACG: Methodology

JC: Investigation, Formal Analysis

NP: Formal Analysis

KV: Investigation

SA: Investigation

HG: Investigation, Writing – Review & Editing

TH: Formal Analysis

KS: Methodology, Writing - Review & Editing

JP: Resources, Writing – original draft, Writing– review & editing, Supervision, Project administration, Funding acquisition

CT: Conceptualization, Resources, Writing – original draft, Writing– review & editing, Supervision, Project administration, Funding acquisition.

AVC: Conceptualization, Resources, Visualization, Writing – original draft, Formal Analysis, Writing– review & editing, Supervision, Project administration, Funding acquisition.

Declarations of interest: none

Word count: 10,429

Keywords: gut-brain axis, Inflammatory bowel disease, gut inflammation, microglia, sex hormones, sexual behaviours, microbiome

Highlights

Early life gut inflammation produces sex-specific i) microbiome, ii) sex hormone and iii) behavioural impacts

Both sexes show disrupted gut bacterial members that regulate sex hormone levels

Male mice demonstrate deficits in mate seeking, which may be mediated by reduced seminal vesicle mass and reduced androgen levels

Female mice lack behavioural deficits, but demonstrate increased amoeboid microglia in the hippocampus

Abstract

Despite recent advances in understanding the connection between the gut microbiota and the brain, there remains a wide knowledge gap in how gut inflammation impacts brain development. Microbiota-derived metabolite signaling from the gut to the brain is required for normal development of microglia, the brain's resident immune cells. Disruption of the microbiota-brain communication has been linked to impaired behaviours and Autism Spectrum Disorder. We hypothesized that intestinal inflammation in early life would negatively affect neurodevelopment through dysregulation of microbiota communication to brain microglia. To test this hypothesis, we developed a novel pediatric model of Inflammatory Bowel Disease (IBD). IBD is an incurable condition affecting millions of people worldwide, characterized by chronic intestinal inflammation, and has comorbid symptoms of anxiety, depression and cognitive impairment. Significantly, 25% of IBD patients are diagnosed during childhood, and the effect of chronic

inflammation during this critical period of development is largely unknown. We developed a chemical model of pediatric chronic IBD by repeatedly treating juvenile mice with dextran sodium sulfate (DSS) in drinking water. DSS-treated mice displayed increased intestinal inflammation, altered microbiota and changes in circulating metabolites. We also found that alterations in gut microbiota had long-term impacts on female microglia and male sex-specific behaviours and testosterone regulation, consistent with delayed puberty observed in male IBD patients. Our research expands our understanding of microbiota-microglia communication underlying development. The gut-brain axis is an exciting target for personalized medicine as microbiome manipulations could be feasible for early intervention to reverse deficits due to juvenile inflammation.

Introduction

Inflammatory bowel disease (IBD) is a group of chronic gastrointestinal (GI) tract conditions that affects over 6.8 million people globally and remains incurable (Alatab et al., 2020). The risk of IBD is correlated with industrialization and, as such, is globally rising in prevalence (Kaplan and Windsor, 2021). Genetic factors account for less than one-third of IBD risk, underscoring the importance of environmental factors such as gut microbiota composition, dietary habits, smoking, and stress levels on disease development (Ananthakrishnan, 2013; Ye et al., 2015). IBD is divided into two subclassifications: Crohn's disease (CD) and ulcerative colitis (UC). CD affects patches of tissue anywhere along the digestive tract, while UC causes continuous inflammation along the colon and rectum (Roda et al., 2020; Torres et al., 2017). Individuals with IBD frequently undergo cycles of intense inflammatory flare-ups and remission periods (Roda et al., 2020). Over 25% of IBD patients are diagnosed during childhood or adolescence

with symptoms that persist through adulthood (Däbritz et al., 2017). Importantly, little is known about the specific impacts of pediatric-onset IBD on the developing brain. Children and adolescents with IBD have an increased risk of developing anxiety and depression, report lower quality of life, and face educational and social challenges in addition to mild cognitive impairments (Attree et al., 2003; Mackner et al., 2013; Thavamani et al., 2019). Furthermore, neuroimaging studies in adult female and male IBD patients have revealed altered brain structure and function (Bao et al., 2015; Lv et al., 2017) some of which correlate with neuropsychiatric impairments (Hou et al., 2020), highlighting the need for similar research in pediatric populations.

Research into inflammatory phenotypes through various animal models – including genetic, chemically induced, and adoptive transfer T cell models – has significantly advanced our understanding of IBD (Wirtz and Neurath, 2007). The widely-used dextran sodium sulfate (DSS)-induced colitis model damages the gut epithelial lining and mimics the gut inflammation and microbiota changes seen in human UC (Chassaing et al., 2014). Adult mice treated with DSS have increased anxiety (Nyuyki et al., 2018) and reduced sucrose preference, indicative of a depression endophenotype (Zhou et al., 2023). Additionally, active gut inflammation in adult mice led to recognition memory impairments in both acute (Emge et al., 2016) and chronic DSS-induced IBD models (Bercik et al., 2011). Importantly, these behavioral deficits were reversed upon resolution of acute inflammation (Emge et al., 2016), which is encouraging for therapeutic resolution of neurophysiological symptons in humans with IBD. While DSS-colitis studies predominantly focus on adult rodents and capture many of the extraintestinal manifestations of IBD seen in adult human patients, research in juvenile rodent models remains limited. In contrast to adult mice, a recent DSS-colitis model in juvenile mice revealed persistent cognitive deficits

and anxiety-like behaviors even upon GI-symptom resolution (Salvo et al., 2020). These observations suggest that GI inflammation during developmental periods may have unique and long-lasting effects on brain development, leading to distinct behavioral impacts in adulthood.

How GI inflammation triggers brain and behavior dysfunction is not well understood, but is theorized to involve altered signaling along the gut-brain-axis. The gut microbiota can signal to the brain by immune cell trafficking, peripheral nerve activity, and release of metabolites that circulate to the brain (Banfi et al., 2021; Günther et al., 2021). One of the key brain cells responsive to gut microbe derived metabolites are microglia, the brain's resident innate immune cells. Microglia sculpt synaptic physiology during brain development (Sullivan and Ciernia, 2022), are acutely sensitive to changes in microbiota in early life (Erny et al., 2015; Thion et al., 2017) and early-life inflammation can chronically alter microglia function (Vogel Ciernia et al., 2018). For example, microbiota-derived short chain fatty acids (SCFAs) can enter the blood stream and cross the blood brain barrier to impact microglia development and function (Cryan and Dinan, 2012; Erny et al., 2015; Sullivan and Ciernia, 2022). In both adult and juvenile IBD mouse models, microglia adopt a pro-inflammatory phenotype characterized by altered cellular morphology and increased pro-inflammatory cytokine secretion (Gampierakis et al., 2021; Salvo et al., 2020; Sroor et al., 2019; Talley et al., 2021). Together, this suggests that early life changes to microbiota-derived signalling to brain microglia may negatively impact brain development in IBD.

Beyond impacting brain function and behavior, pediatric IBD poses several unique challenges in other aspects of development, including delayed onset of puberty in both males and females (Ballinger et al., 2003). While undernutrition was inititally thought to be the main driver of delayed puberty, restoring nutritional status fails to normalize the timing of puberty onset,

suggesting the involvement of additional factors (Azooz et al., 2001; Brain and Savage, 1994; DeBoer et al., 2010; Deboer and Li, 2011). Specifically, numerous studies have identified inflammation and altered sex hormone regulation as critical mechanisms involved in delayed puberty onset among IBD patients. For instance, animal models of IBD have linked intestinal inflammation to disruption in testosterone levels, estrogen receptor function, and reproductive organ size, with effects that extend beyond what is seen with undernutrition alone (Azooz et al., 2001; Ballinger et al., 2003; DeBoer et al., 2010; Deboer and Li, 2011) . Similarly, findings in human studies show that IBD patients can have disrupted sex hormone levels (Klaus et al., 2008; Tigas and Tsatsoulis, 2012) and higher rates of sexual dysfunction (Chen et al., 2024; Gaidos et al., 2020). A connection between inflammation and altered hormone levels is thought to be mediated by the gut microbiota, which acts as a regulator of estrogen and androgen synthesis and metabolism (Colldén et al., 2019; He et al., 2021; Maffei et al., 2022; Neuman et al., 2015). In mouse models of IBD, the loss of bacterial species such as *Faecalibacterium prausnitzii* (Sokol et al., 2008) and *Roseburia hominis*, known for producing anti-inflammatory SCFAs, is associated with changes in sex hormone levels (Sui et al., 2021; Torres et al., 2018). The depletion of specific bacteria such as *F. prausnitzii* in IBD, which are crucial for converting estrogen to its active form, can directly impact hormone availability, potentially affecting the onset and progression of sexual development (Ervin et al., 2019). Additionally, the recent discovery of testosterone-degrading bacteria such as *Mycobacterium* contributing to inflammation in IBD underscores the microbiota's profound impact on male and female sexual development, suggesting avenues for targeted microbial interventions to mitigate impairments in IBD (Li et al., 2022; Naser et al., 2014). These studies highlight the complex interplay between the gut microbiota and sexual development (Lavelle and Sokol, 2020; Machiels et al., 2014).

Altogether, there is currently a critical gap in understanding the complex interplay between early life intestinal inflammation, brain function and reproductive development. To bridge these gaps, we introduce a mouse model of pediatric-onset IBD that captures recurrent episodes of gut inflammation throughout childhood and adolescence, modeling the human condition. In both sexes, we assessed the acute and chronic effects of early-life gut inflammation on gut microbiota composition, short-chain fatty acid production, a wide variety of behaviors, sex steroid levels, brain white matter tract integrity and microglial morphology, offering a comprehensive view of IBD's impact on juvenile development. Our findings reveal novel sex-specific changes in reproductive behavior, alterations in microbiota metabolites and hormone signaling, and microglial morphology adaptations. These results highlight the unique long-term consequences for human patients with early-onset IBD, emphasizing a need for early diagnosis and microbiome-targeted intervention strategies.

Methods

Animals

Experimentally naïve 3-week-old C57BL/6J wildtype mice (strain #000664, Jackson Laboratories) were housed in groups of 3-5 with sex and treatment-matched cage mates. Mice were housed under a 12:12 light-dark cycle with lights on at 0700h and lights off at 1900h in a temperature (22ºC) and humidity (40-60%) controlled environment. Purina LabDiet 5k67 diet and water were given *ad libitum* throughout the experiment unless stated otherwise for specific tasks. All housing conditions and testing procedures were in accordance with the guidelines of the Canadian Council on Animal Care, and all protocols were approved by the Animal Care

Committee of the University of British Columbia *(protocols A19-0078, A23-0115, and A23-0086)*.

Pediatric IBD mouse model

Mice randomly assigned to the treatment groups were administered three rounds of 5-day treatments of 3-3.5% colitis-grade DSS(36-50 kDa, MP Biomedicals #160110) while the vehicle control group (VEH) received autoclaved distilled water. The treatment periods occurred during postnatal days (P) P21-26, P42-47, and P63-68 (Figure 1A). During treatment and for three days following each treatment, mice were weighed daily to monitor for weight loss. Regular monitoring of weight was continued during the recovery period intervals. One cohort of mice was euthanized three days after the final DSS treatment on P71 (n=4-5/treatment/sex). The remaining two cohorts of mice underwent behavioral testing as young adults between P85-P130 (n=11-13/treatment/sex).

Serum and organ collection

Animals were deeply anesthetized with 5% isoflurane, and blood was collected by cardiac puncture. Whole blood was collected into BD Microtainer™ Serum Separator Tubes (BD) and allowed to coagulate for at least 30 minutes at room temperature according to manufacturer instructions. To isolate serum for later analyses, blood samples were spun down at 1200 x g for 20 minutes at 4ºC, and the serum was removed and placed in a new tube for storage at -80ºC. Animals were then transcardially perfused with 1X phosphate buffered saline (PBS). Intestinal measures were conducted as follows: first, intestines were dissected out from the gastroduodenal junction to the rectum. Colon length was then measured from the ileocecal junction to the rectum. The contents of the cecum were gently scraped and collected into a sterile tube, then

immediately flash-frozen on dry ice. The colon was manipulated into rolls in histological cassettes and immediately fixed in freshly prepared Methacarn solution (60% dry methanol, 30% chloroform, 10% glacial acetic acid) (Ng and Tropini, 2021). Brains were collected and drop fixed in 4% paraformaldehyde (PFA) for 24 hours at 4°C and then transferred to 30% sucrose solution and kept at 4°C until sectioned. For brain connectivity analysis, mice were perfused with PBS followed by 4% PFA and brains were dissected out and then stored in 4% PFA until scanning.

Gut staining and histological scoring

Within 2 weeks of fixation in Methacarn solution, intestinal tissues were processed and infiltrated with paraffin wax as previously described (Ng and Tropini, 2021). Briefly, tissues were washed twice with absolute methanol for 30 minutes each, followed by two washes with absolute ethanol for 20 minutes each. Next, tissues were washed twice with xylene for 15 minutes before being placed in melted paraffin wax and incubated for 2 hours at 60ºC. Samples were then sent to the BC Children's Hospital Histology Core for embedding in paraffin wax and sectioning into 4 – 5 µm sections. Histological staining was performed with hematoxylin and eosin as previously described (Stahl et al., 2017). Finally, slides were imaged using a PANNORAMIC® MIDI II (3DHISTECH).

Mucus and bacteria visualization

Visualization of gut microbes was performed as previously described (Ng and Tropini, 2021). Briefly, to deparaffinize tissues, slides were heated at 60ºC in Coplin jars for 10 minutes, followed by incubation in xylene that was pre-warmed to 60ºC. A second xylene wash was performed at room temperature for 10 minutes, then slides were placed in 99.5% ethanol for 5

minutes. After allowing slides to air-dry, tissues were encircled using a liquid blocker PAP pen. FISH probe hybridization solution (20 mM Tris-HCl, pH 7.4; 0.9 M NaCl; 0.1% sodium dodecylsulfate in nuclease-free water) was pre-warmed to 50ºC before addition of Eub-388 (5'-AF488-GCTGCCTCCCGTAGGAGT-3') to a final concentration of 10 ng/µL (Amann et al., 1990). Slides were then incubated for 3 hours at 50ºC in a humid chamber. Following incubation, tissues were washed once with FISH washing buffer (20 mM Tris-HCl, pH 7.4; 0.9 M NaCl, pre-warmed to 50ºC) for 10 minutes at 50ºC, then additionally with 1x PBS. DNA and intestinal mucus were counter-stained using 10 µg/mL DAPI and 40 µg/mL UEA-1-Rhodamine Red respectively in PBS for 45 minutes at 4ºC. Finally, slides were washed thrice with PBS before mounting with ProLong Gold AntiFade mounting medium (Invitrogen). Fluorescence images were captured using a Zeiss LSM900 confocal microscope using a 100x objective lens.

Microbiome sequencing and analysis

Microbiome composition was determined via sequencing of the 16S rRNA hypervariable region. Total DNA was extracted from 30-60 mg of cecal contents using the DNeasy PowerSoil Pro kit (Qiagen) in accordance with manufacturer protocols. Quantification of extracted DNA concentration prior to library preparation was performed using the Quant-iT™ dsDNA HS Assay (Thermo Fisher). 16S library preparation was conducted at either the Gut4Health facility at BC Children's Hospital or the Biofactorial High-Throughput Biology (Bio!) Facility at the University of British Columbia. For samples collected 3 days after cessation of DSS, library preparation targeting the V4 hypervariable region of the 16S rRNA gene was performed at the Gut4Health facility using established protocols (De Wolfe and Wright, 2023). Amplification of the V4 region was performed with 515F/926R primers (515F, 5'-GTGYCAGCMGCCGCGGTAA-3'; 926R, 5'-CCGYCAATTYMTTTRAGTTT-3'). Pooled

libraries were then submitted to the Bio! facility, where sequencing was performed on the Illumina MiSeq™ platform with v2 2 x 250 bp paired-end read chemistry. For all other samples, library preparation targeting the V4-V5 16S rRNA genes was performed at the Bio! Facility as previously described (Ng et al., 2023), and sequencing was run on the Illumina MiSeq™ platform with v3 2 x 300 bp paired-end read chemistry. FASTQC (Andrews, 2010) was run on the generated FASTQ files to assess read quality. Reads were then imported into QIIME2-2023.2 for subsequent analyses (Bolyen et al., 2019). Denoising and quality filtering was performed using DADA2 (via q2-dada2), and reads were trimmed to remove primer sequences while maintaining mean Phred quality scores >Q30 (Callahan et al., 2016). Multiple sequence alignment and phylogenetic tree generation was performed using MAFFT (via q2-alignment) and FastTree2 respectively (via q2-phylogeny) (Katoh et al., 2002; Price et al., 2010). Using the QIIME classification plugin (q2-feature-classifier), amplicon sequence variants (ASVs) were classified via a naïve Bayes machine-learning taxonomic classifier against the SILVA 138 99% identity reference sequence database (Quast et al., 2013).

Further analyses were conducted using R v4.2.2 (R Core team, 2021). Analyses were visualized through the tidyverse (Wickham et al., 2019) and ggplot2 (Hadley, 2016) packages. For sample rarefaction, calculation, and visualization of alpha and beta diversity metrics, the phyloseq (McMurdie and Holmes, 2013), ggpubr (Kassambara, 2023), and vegan (Dixon, 2003) packages were employed. Differential abundance analysis (DAA) was conducted using the ANOVA-Like Differential Expression (ALDEx2) (Gloor et al., 2023) and Analysis of Composition of Microbiomes (ANCOM) (Mandal et al., 2015) packages through the microbiomeMarker package (Cao et al., 2022). The relative abundance of those taxa identified as significantly differentially abundant were then plotted with p-values obtained with ALDEx2. Differentially abundant taxa

were plotted using the ComplexHeatmap (Gu et al., 2016) package. The relative abundance of select differentially abundant taxa was then plotted against serum hormone concentrations, and Spearman's correlation was calculated using smplot2 (Min and Zhou, 2021).

Behavior testing

All behavior testing was performed under white light (600 lux) between the hours of 0900-1800 except for the sucrose preference test, which is a 24-hour task. Animals were habituated to the researchers after the anxiety tasks but prior to all other tests through 3 days of handling (1-2 min/mouse). For each behavior task, animals were first habituated to room conditions for 30 minutes before testing. For all tasks that did not involve bedding, the apparatus was cleaned with diluted saber solution (Vert-2-Go saber diluted 1:16 in water) between mice and between stages. ANY-maze tracking software (Stoelting) was used to record videos and track animal movement during the task. Mice began testing 17 days following the final round of DSS (n=11-13/treatment/sex) with the exception of a subset cohort, which underwent only the urine preference test and mating behavior test beginning 28 days following the final round of DSS treatment (n=7-8/treatment/sex).

<u>Urine Preference Test (UPT)</u>

Mice were placed in the centre of an open-top box (40 cm x 40 cm x 40 cm, L x W x H) containing two 10 cm diameter inverted pencil cups in opposite corners. Under each pencil cup was a petri dish with blotting paper (1 cm^2). Mice were given a 10-minute habituation period where 20 µL of deionized water was dropped onto both blotting papers. Following habituation, mice were given another 10-minutes to explore the two cups, this time with 20 µL of pooled

male or female C57BL/6 mouse urine dropped onto one of the blotting papers and 20 μL of deionized water dropped onto the other. In the final stage, mice were given another 10-minutes to explore the two cups, with the urine cup location and urine sex switching from the previous stage (Malkesman et al., 2010). Presentation order of same or opposite sex urine as well as location of urine in the first and second stages was counterbalanced across mice and treatment conditions. ANY-maze tracked the total investigation time, counted when the test mouse nose was within 1cm of the inverted pencil cup. Exclusion criteria for data collected during the urine preference test include side preference during habituation (defined as a discrimination index (DI) over 20 or under -20, where DI is the difference in time spent investigating the stimulus cups divided by the total time spent investigating) and side preference exceeding three standard deviations from the mean.

Mounting Behavior

Sexually inexperienced VEH- and DSS-treated male mice were paired with a novel sexually experienced C57BL/6 female mouse in an empty 35 cm x 20 cm x 15 cm clear plastic box. ANY-maze (Stoelting) was used to record a 15-minute free interaction period. Videos were hand-scored for the frequency and duration of male mounting by a researcher blind to treatment conditions. Mounting behavior was defined as male contact with two paws on the front or back of the female as previously described (Bayless et al., 2023).

Open Field Test

The open field was performed in an open-topped grey Plexiglass arena (65 cm x 65 cm x 40 cm; L x W x H). Mice were placed in the centre of the arena and given 20 minutes to freely explore. ANY-maze tracked the total distance traveled and the amount of time spent in the inner and outer zones. The outer zone was defined at 8 cm from the wall of the apparatus.

Elevated Plus Maze

The plus-shaped apparatus was elevated 50 cm above the floor and had two open arms and two closed arms, both 30 cm x 8 cm (L x W). The closed arms were surrounded by 15 cm high walls. Mice were placed in the centre of the apparatus and allowed to freely explore for 5 minutes. ANY-maze tracked the total distance traveled and the amount of time spent in the open arms and closed arms.

Three Chamber Test

The test apparatus was an open-topped rectangular box (60 cm x 40 cm x 22 cm ; L x W x H) divided lengthwise into three identically sized compartments (Yang et al., 2011). The task consisted of three 10-minute phases: habituation, sociability, and social novelty. The sociability and social novelty phases require sex and age matched stimulus mice. Prior to the task, stimulus mice spent 20 minutes/day for 3 days habituating to sitting under inverted pencil cups.

During the first (habituation) phase, experimental mice were placed in the middle compartment of the apparatus and allowed to freely explore all areas of the chamber. In the sociability phase, a sex and aged matched stimulus mouse was placed under a 10 cm diameter inverted pencil cup on one side of the apparatus. The other side contained just an empty inverted pencil cup. Both cups had cylindrical weights placed on them to prevent mice from climbing on top of the cups or pushing them. In the social novelty phase, the sociability-phase stimulus mouse became the ‘familiar’ mouse, and a second ‘novel’ sex and aged matched mouse was introduced under the previously empty pencil cup. The novel mouse was not a cage mate of the familiar mouse. In between stages experimental mice were confined to the centre chamber while the stimulus mouse was placed under the cup.

ANY-maze was used to track distance traveled, time in each chamber, and time spent investigating the cup in each phase of the task. When the mouse's nose was within 1 cm of the pencil cup and pointing directly at it, investigation was scored. Looking over or past the cup and climbing on top of the object were not counted as investigation.

Olfaction Habituation-Dishabituation Test

The olfaction test was performed as previously described (Yang and Crawley, 2009). Briefly, mice were habituated to a clean cage without bedding for 30 minutes prior to being repeatedly presented a cotton swab with various social and non-social odors. Mice were presented with each scent three times for 2 minutes, with a 1-minute break between each odor presentation. The non-social odors (vanilla or banana extract) were prepared diluted 1:100 in deionized water. The social odors were collected by wiping the cotton swab in a zig-zag pattern along the bottom of the cage of either same-sex or opposite-sex mice. The order of odor presentation was: water, vanilla extract, banana extract, same sex mice, opposite sex mice. Videos were recorded and hand-scored by researchers blinded to experimental conditions for the time spent investigating each odored cotton swab, defined as the nose within 1 cm of the swab. Biting and otherwise playing with the cotton swab was not counted as olfaction investigation.

Object Location Memory (OLM) Test

The OLM test was performed in an open-topped Plexiglass square box (40 cm x 40 cm x 40 cm ; L x W x H) lined with bedding ~1 cm in depth. Bedding was kept in the same box each day. One wall of the box was lined with duct tape as a visual cue. Objects were cleaned with diluted saber solution between trials and allowed to fully dry before re-use.

The OLM took 8 days in total with 6 days of habituation, 1 day of training and 1 day of testing (Vogel-Ciernia and Wood, 2014). Mice were habituated for 10 minutes for 6 days, where they were allowed to freely explore the box with no objects present. On the training day, mice were given 10 minutes to investigate two identical cylindrical spice tins filled with cement as described previously (Vogel-Ciernia and Wood, 2014). The 5-minute testing phase took place 24 hours after training. During the test, one object was moved to a novel location and the other remained in the original training location.

ANY-maze tracked the total distance traveled on all 8 days. ANY-maze tracked investigation time and the number of investigations of each object on training and testing days. Investigation time was scored when the mouse's nose was within 1 cm of the object and pointing directly at the object. Looking over or past the object and climbing on top of the object were not counted as investigation. For the training and testing days, a discrimination index (DI) was calculated where DI is the difference in time spent investigating the moved object and the unmoved object divided by the total time spent investigating both objects x100.

Mice who had a DI over 20 or under -20 during the training phase were determined as having an innate preference and excluded from final analysis. Mice who explored the objects more or less than 3 standard deviations from the mean were also excluded from analysis as we have done previously (Vogel-Ciernia and Wood, 2014).

Self-Grooming and Forced Grooming

Mice were individually placed in a new cage without bedding. After a 5 minute habituation period, the cumulative time spent naturally self-grooming was recorded for 5 minutes. The mice were then lightly sprayed with water from a mist bottle and forced self-grooming was scored in

the following 5 minutes. All hand scoring of grooming behavior was performed by a researcher blinded to experimental conditions.

Forced Swim Test

Mice were placed individually into 1 L glass beakers filled with 900 mL of water at a temperature of 23-25°C. Mice were recorded for 6 minutes and then removed from the water. Mice were placed in a cage with dry paper towel on top of a heating pad after the task and were returned to the home cage once they were dry and exhibiting normal motor and grooming behaviors. The last 4 minutes of footage was hand-scored for time spent immobile, defined as the absence of escape-related movements. The hand-scorer was blind to experimental conditions.

Sex steroid quantification

Serum (10 µl) was pipetted into 2 mL polypropylene bead ruptor tubes with 5 ceramic zirconium oxide beads (Hamden, et al. 2021a; Hamden, et al. 2021b; Tobiansky, et al. 2018). Calibration curves (0.05 – 1000 pg), blanks, and quality controls were extracted alongside samples via liquid-liquid extraction and analyzed by specific and ultrasensitive LC-MS/MS as before (Hamden et al. 2021a). Progesterone, testosterone (T), androstenedione (AE), 5α-dihydrotestosterone (DHT), and 17β-estradiol (E_2) were measured using multiple reaction monitoring with 2 mass transitions for each analyte (Hamden, et al. 2021a; Hamden, et al. 2021b; Tobiansky, et al. 2018). Deuterated internal standards (progesterone-d9, testosterone-d5, and 17β-estradiol-d4) were included in all standards, blanks, controls, and samples to correct for analyte loss and matrix effects. Steroid concentrations were acquired by a Sciex 6500 Qtrap triple quadrupole tandem mass spectrometer. A steroid was considered non-detectable if either the quantifier or qualifier transition was not present. If 50% or more of the values in a group

were detectable, then missing values were replaced with the lower limit of quantification/√2 (Handelsman and Ly 2019). DHT and E_2 were non-detectable in all samples, and AE was non-detectable in all female samples.

Brain microglia immunofluorescence staining

After PFA fixation and sucrose cryoprotection, brain hemispheres were embedded in Optimal Cutting Temperature (OCT) compound (Scigen, 23-730-625), cryosectioned at 30 µm, and stored in 1X PBS at 4°C. For staining, free-floating sections were permeabilized with 1X PBS + 0.5% Triton X-100 for 5 minutes and then washed 3 x 5 minutes with 1X PBS. Sections were placed in a blocking solution (5% normal donkey serum, and 1% bovine serum albumin dissolved in 1X PBS + 0.03% Triton) for 1 hour at room temperature with gentle shaking and then incubated with anti-IBA1 primary antibody (chicken; Synaptic Systems (234009); 1:1000) for 48 hours. Sections were washed 3 x 5 minutes in 1X PBS + 0.03% Triton and then incubated in a donkey anti-chicken secondary antibody (Alexa Fluor® 488 Jackson ImmunoResearch (703545185); 1:500) and DAPI (Biolegend (422801); 1:1000) for two hours at room temperature on a gentle tilt. Sections were washed 3 x 5 minutes in 1X PBS + 0.03% Triton and 1x 5 minutes in 1X PBS and then mounted onto glass slides and coverslipped using Invitrogen ProLong Glass Antifade Mountant (Invitrogen, P36984).

Microglial morphology analysis

Slides were imaged using the Zeiss Axioscan7 slide scanner microscope at 20X magnification. Maximum intensity extended depth of focus (EDF) images were acquired from Z-stacks containing 16 slices at a step size of 1 µm. EDF images were created using maximum projection settings and converted to tiffs using ZEN (Zeiss). Maximum projection EDF images compile the

pixels of highest intensity at any given z-stack position and construct a new 2D image retaining the 3D information. The hippocampus and hypothalamus anatomical regions were traced using the FASTMAP FIJI plugin with reference to the Allen Brain Atlas (Terstege et al., 2022). Within these segmented regions, microglial morphology was analyzed using the pipeline described in Kim et al., 2023 using MicrogliaMorphology (ImageJ tool) and MicrogliaMorphologyR (R package) which uses Image-J plugins Skeletonize (2D/3D) and AnalyzeSkeleton (2D/3D)(Arganda-Carreras et al., 2010) to collect 27 metrics of morphology per microglial cell (Supplemental Figure 3A). We conducted dimensionality reduction using principal component analysis followed by k-means clustering on the first three principal components (Supplemental Figure 3C) to define four morphological classes within our dataset (hypertrophic, rod-like, ramified, ameboid). We identified the optimal clustering parameter using exploratory data analysis methods including the within sum of squares and silhouette methods (Supplemental Figure 3B). We assigned cluster identities by examining the relationship between each cluster and the 27 morphological features (Supplemental Figure 3D) and by using the ColorByCluster feature in MicrogliaMorphology to visually examine the different cluster morphologies (Figure 7A).

We then calculated the percentage of cells in each morphology cluster for each treatment and sex using the 'clusterpercentage' function within MicrogliaMorphologyR. To assess how cluster membership changes with treatment for each sex, we fit a generalized linear mixed model using a beta distribution to model the percentage of cluster membership as a factor of Cluster identity and DSS treatment with MouseID as a repeated measure ("percentage ~ Cluster*treatment + (1|MouseID)") using the `stats_cluster.animal` function from MicrogliaMorphologyR, which is wrapped around the glmmTMB R package (Brooks et al., 2017). We ran a 2-way Analysis of Deviance (Type II Wald chisquare test) test on the model to assess the contribution of Cluster and treatment interactions. Tests between treatment

conditions were corrected for multiple comparisons across Clusters (~treatment|Cluster) using the Sidak method and q-values < 0.05 were considered statistically significant.

Short and medium chain fatty acid quantification

Serum samples were stored in -80 freezer prior to lipid extraction. A total of 50 µL of serum was mixed with 450 µL ice-cold methanol, vortexed for 10 seconds, and incubated at -20 ºC for 4 hours for protein precipitation. Samples were then centrifuged at 14,000 rpm at 4 ºC for 15 minutes, and the supernatant were collected and dried down via SpeedVac at 4 ºC. The dried extract was reconstituted in 100 µL of water and acetonitrile solution (1:1, v:v) for LC-MS analysis. Quality control (QC) samples were prepared by pooling 20 µL aliquot from each sample to monitor the instrument performance and optimize the injection volume. A method blank sample was prepared using the identical analytical workflow but without serum. An UHR-QqTOF (Ultra-High Resolution Qq-Time-Of-Flight) Impact II (Bruker Daltonics, Bremen, Germany) mass spectrometry interfaced with an Agilent 1290 Infinity II Ultrahigh-Performance Liquid Chromatography (UHPLC) system (Agilent Technologies, Santa Clara, CA, USA) was used for analysis. LC separation was achieved using a Waters reversed phase (RP) UPLC Acquity BEH C18 Column (1.7 µm, 1.0 mm ×100 mm, 130 Å) (Milford, MA, USA) maintained at 25 °C. The mobile phase A was 5% ACN in H_2O with 10 mM ammonium acetate (pH = 9.8, adjusted ammonium hydroxide) and the mobile phase B was 95% ACN in H_2O. The LC gradient was set as follow: 0 min, 5% B; 8 min, 40% B; 14 min, 70% B; 20 min, 95% B; 23 min, 95% B; 24 min, 5% B; 33 min, 5% B. The flow rate was 0.1 mL/min. Negative ion mode was applied with the following MS settings: dry gas temperature, 220 °C; dry gas flow, 7 L/min; nebulizer gas pressure, 1.6 bar; capillary voltage, 3000 V. External calibration was applied using sodium formate to ensure the *m/z* accuracy before sample analysis.

SCFA and MCFA measurements from cecal contents were obtained as follows. In brief, 20-40 mg of cecal contents were mixed with 0.4 – 0.8 mL of 25% phosphoric acid in water (LabChem). Sample mixtures were thoroughly homogenized via vortexing, then centrifuged at 15,000 x g for 10 minutes at 4ºC. Following centrifugation, the sample supernatant was transferred to a new tube, then centrifuged again at 15,000 x g for 10 minutes at 4ºC. The resulting supernatant was then frozen at -20ºC before being sent to the University of Alberta AFNS Chromatography Facility for volatile fatty acid (VFA) analysis using gas chromatography/mass spectrometry (GC/MS) as previously described (Ng et al., 2023). There, the supernatant was filtered through 0.45 µm filters and mixed in a 4:1 ratio with internal standard solution (24.5 mmol/L isocaproic acid). The samples were then injected into a Stabilwax-DA column (length: 30 m, inner diameter: 0.53 mm, film thickness: 0.5 µm, Restek Corporation) on a Bruker Scion 456 GC with a model 8400 autosampler (Bruker Ltd) using a helium carrier gas. The samples were run using a 10 mL/min constant flow with a 5:1 split ratio with a column temperature gradient as follows: 80ºC initial temperature, immediately increased to 180ºC at 20ºC/min, then held for 3 min at 180ºC. The injector and detector temperature were at 250ºC. The peaks were analyzed using CompassCDS software. The concentration of SCFAs/MCFAs per sample was then normalized to mass of the cecal contents for statistical testing.

MRI acquisition and data processing

Ex vivo imaging and analysis, including standard data preprocessing and region of interest (ROI) analyses, were performed as previously described (Yi et al., 2019). Briefly, brains were extracted from the cranial vault between P95 and P130 and post fixed in 4% PFA (n = 54;13 vehicle per sex, 14 DSS per sex). Brains were placed in a custom-built holder immersed in Fluorinert (FC-3283, 3M, St. Paul, MN, USA) and imaged with a 4.7-T Agilent MRI system with a 3.5 cm

diameter quadrature volume RF coil. Multi-slice, diffusion-weighted, spin echo images were used to acquire 10 nondiffusion weighted images (b=0 s•mm^{-2}) and 75 diffusion-weighted images (25: b=800 s•mm^{-2}, 50: b=2,000 s•mm^{-2}), using non-colinear diffusion-weighting directions. Diffusion imaging was performed with a TE/TR=24.17/2000-ms, FOV=30×30 mm^2, and a matrix=192×192 reconstructed to 256×256 for an isotropic voxel size of 0.25-mm over two signal averages. Raw data files were converted to NIfTI format and FSL was used to correct for eddy current artifacts (Smith et al., 2004). A DTI-based mouse brain atlas (Jiang and Johnson, 2011) was used as a study space template and to define regions of interest (ROI) including the left and right hippocampus, frontal association cortex, striatum, amygdala, thalamus, and hypothalamus. Multi-shell diffusion data were fit with the Microstructure Diffusion Toolbox (MDT) (Harms et al., 2017) to the neurite orientation dispersion and density imaging (NODDI) model (Zhang et al., 2012). An additional compartment of isotropic restriction was included to account for potential fixative effects as recommended (Alexander et al., 2010). The mean values for neurite density index (NDI) and orientation dispersion index (ODI), which represent indices of intracellular and extracellular diffusion respectively, were calculated in each ROI using Pyradiomics (van Griethuysen et al., 2017) and compared among experimental groups.

Statistical analyses

Statistics and graphs were created with GraphPad Prism 9.5.1 (GraphPad Software) and RStudio software (RStudio Team, 2022). A repeated measures ANOVA was used to assess body weight changes during treatment. All organ comparisons, SCFA measurements, and almost all behavioral tests were assessed using a two-way ANOVA to assess main effects of treatment and sex and Šidák corrected post-hoc comparisons were performed to determine statistical significance within sex if main effects or interactions were observed. The urine preference test

was assessed by comparing each group to chance (50%) using a single sample t-test. To directly compare preferences between treatments, an unpaired two-tailed t-test was conducted. Steroid levels were analyzed by Mann-Whitney U. Statistical significance of alpha diversity metrics (Observed features) was assessed using a two-way ANOVA to assess main effects of treatment and sex. Beta diversity metrics were evaluated using PERMANOVA analysis. P-values obtained from DAA with ALDEx2 were reported.

For the MRI analysis, a 2 × 2 analysis of variance (ANOVA) was used to determine the effect of treatment, biological sex, and their interactions on the ROI values. The effects of ROI laterality and imaging age effects were regressed from the data before the ANOVA was performed as these effects were not pertinent to the tested hypotheses. Benjamini-Hochberg false discovery rate (FDR) procedure was used to control for multiple hypothesis testing across ROIs within each imaging signal. Statistical significance of an ANOVA is defined as an FDR adjusted p-value <0.05. Post-hoc pairwise difference testing was performed using Fisher's LSD test Partial η^2 explains how much of the unexplained variance in the model is described by the addition of that variable into the model. The plotted imaging metric values represent the metric values after the laterality and batch effects have been removed. All statistical analyses were performed using GraphPad Prism 10.1.1 (GraphPad Software) and Python 3.8 with package statsmodel.

Results

An early-life DSS model of pediatric IBD

To establish a model of juvenile-onset IBD that mimics the remitting and recurrent cycles of gut inflammation often observed in IBD patients, we set out to optimize a chemical model of colitis to both target the juvenile age range and emulate repeated cycles of inflammation. Previously,

Salvo et al. modeled pediatric IBD by administering 2% DSS for 5 days at weaning (P21) as a model of a single acute period of inflammation (Salvo et al., 2020). Studies in adult rodents have utilised several rounds of DSS to emulate recurring cycles of inflammation and remission (Eichele and Kharbanda, 2017; Okayasu et al., 1990; Zhou et al., 2023). Therefore, we adapted a model in which DSS is administered in the drinking water repeatedly across early postnatal development starting at postnatal day 21 (P21) (Ruemmele and Turner, 2014).

Starting on P21, 3 rounds of DSS were administered for 5 days followed by 2 weeks of recovery; control mice (VEH) received water throughout (Figure 1A). Colon length is indicative of inflammatory state, with colon shortening being induced by effective DSS treatment (Chassaing et al., 2014). Three days after the final treatment, colon length was significantly decreased by DSS in both sexes (main effect of treatment ($F(1, 21) = 39.30$, $p<0.0001$) (Figure 1B). Both female ($p=0.009$) and male ($p=0.0002$) mice treated with DSS had colon lengths that were significantly shorter than untreated mice, indicating successful induction of intestinal inflammation in our model. Furthermore, body weights were recorded throughout the treatment period (Chassaing et al., 2014) (Figures 1C, D). Female mice showed mild weight loss in response to DSS, with only the second round producing significant decreases from VEH littermates (treatment x day interaction $F(50,714) = 6.693$, $p<0.0001$) (Figure 1C). Conversely, male DSS-treated mice showed more dramatic weight loss across the three treatment periods (treatment x day interaction $F(50,686) = 12.372$, $p<0.0001$) (Figure 1D). To further investigate inflammation caused by repeated administration of DSS, we examined the histological architecture of colonic tissues using hematoxylin and eosin staining. Following chronic DSS treatment, the gut epithelial layer was disturbed, showing increased crypt length (crypt abscess), depletion of mucus-producing goblet cells, increased incidence of inflammatory cell infiltration,

and ruffling of the normally smooth epithelium (Ng and Tropini, 2021) (Figures 1E, F). Furthermore, UEA-1 lectin staining targeting the intestinal mucus layer revealed that DSS-treated juvenile mice experienced profound alterations in mucus structure, with loss of the striated bilayer organization (Figure 1F). Finally, to examine changes to gut microbiota composition caused by repeated cycles of early life inflammation, we performed 16S rRNA sequencing targeting the bacterial V4-V5 variable regions. Consistent with previous studies in adult mice, DSS treatment resulted in significant losses to microbiota alpha diversity, with the number of observed features, a proxy for the number of bacterial species present (Kleine Bardenhorst et al., 2022), being significantly decreased in DSS-treated animals compared to vehicle (significant effect of treatment $F(1,12) = 5.3$, $p = 0.0387$) (Figure 1G) (Munyaka et al., 2016). Similarly, between-group microbiota compositional differences were revealed to be significantly different when compared using calculated Bray-Curtis distance matrices (treatment x sex interaction $F(1,12) = 3.2158$, $p<0.046$) (Figure 1H). Altogether, these results suggest that our DSS colitis model of juvenile IBD induces profound physiological and microbiological changes to the gut.

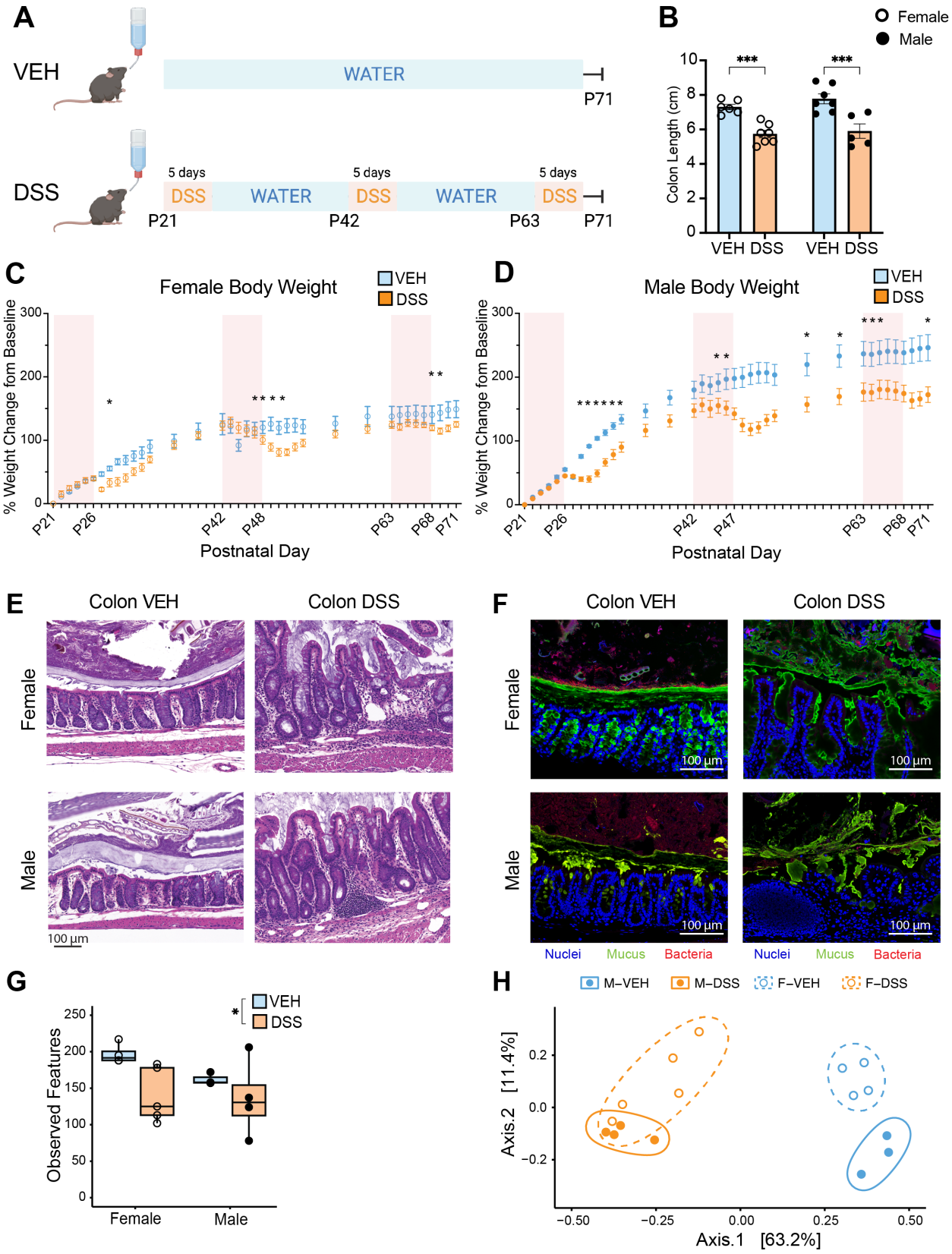
A
VEH
WATER
P71
DSS
5 days
DSS
WATER
5 days
DSS
WATER
5 days
DSS
P21
P42
P63
P71
B
Female
Male
Colon Length (cm)
***
***
VEH DSS
VEH DSS
C
Female Body Weight
VEH
DSS
% Weight Change fom Baseline
Postnatal Day
P21
P26
P42
P48
P63
P68
P71
D
Male Body Weight
VEH
DSS
% Weight Change fom Baseline
Postnatal Day
P21
P26
P42
P47
P63
P68
P71
E
Colon VEH
Colon DSS
Female
Male
100 µm
F
Colon VEH
Colon DSS
Female
Male
100 µm
Nuclei
Mucus
Bacteria
G
VEH
DSS
Observed Features
Female
Male
H
M–VEH
M–DSS
F–VEH
F–DSS
Axis.2 [11.4%]
Axis.1 [63.2%]

Figure 1. Juvenile mouse DSS treatment models early life intestinal inflammation. *A*. Experimental schematic. Control mice were given water throughout (VEH), while treatment mice were given 3 rounds of 5-day long DSS treatments beginning at P21, P42, and P63 (DSS). *B.* Post-treatment colon lengths measured at P71, three days after the final round of DSS is shorter in DSS treated mice. Each graph bar and error bar represent the mean ± SEM. *C, D.* Female and male percent weight change from baseline (P21) starting weight. Each point and error bar represents the mean ± SEM. *E.* Representative images of hematoxylin and eosin-stained colonic tissues from mice collected at P71 confirm that DSS treatment induced intestinal inflammation. Scale bar, 0.100 mm. *F.* Representative fluorescence *in situ* hybridization (FISH) images from VEH and DSS treated mice shows gut disruption in DSS treated mice. Scale bar, 100 µm. Colours: host tissue (DAPI, blue), mucus (UEA-1, green), and bacteria (Eub-338, red). *G.* Microbiota alpha diversity as measured by number of observed unique features (a proxy for number of species) per sample is significantly lower in DSS treated mice *H.* Principal Component Analysis of Bray-Curtis diversity index shows separation by DSS treatment. *$p<0.05$. ***$p<0.0001$.

Early-life DSS affects self-grooming behavior in male mice

Previous work in early life gut-inflammatory models, including those for IBD and autism spectrum disorders, identified altered mouse behavior (Salvo et al., 2020). To fully profile any behavioral phenotypes in our pediatric IBD model, we performed a battery of behavioral testing beginning 17 days after DSS treatment to examine anxiety (elevated plus maze, light-dark box, open field test), memory (spatial object location), sociability and social memory (three chamber

task), repetitive behavior (self-grooming), and depression-like behaviors (forced swim and tail suspension tests). Unlike previous reports, we did not observe any significant effects of treatment for either sex in most of these tests (Figure 2 and Supplemental Table 1), with the single exception of decreased self-grooming (main effect of treatment ($F(1, 24) = 6.514$, $p=0.018$) in the DSS-treated males ($p=0.031$). This suggests that that the majority of behaviors examined are not impacted by previous repeated bouts of postnatal gut inflammation in early-life, potentially due to the normal development of most neuronal circuits prior to treatment beginning at P21.

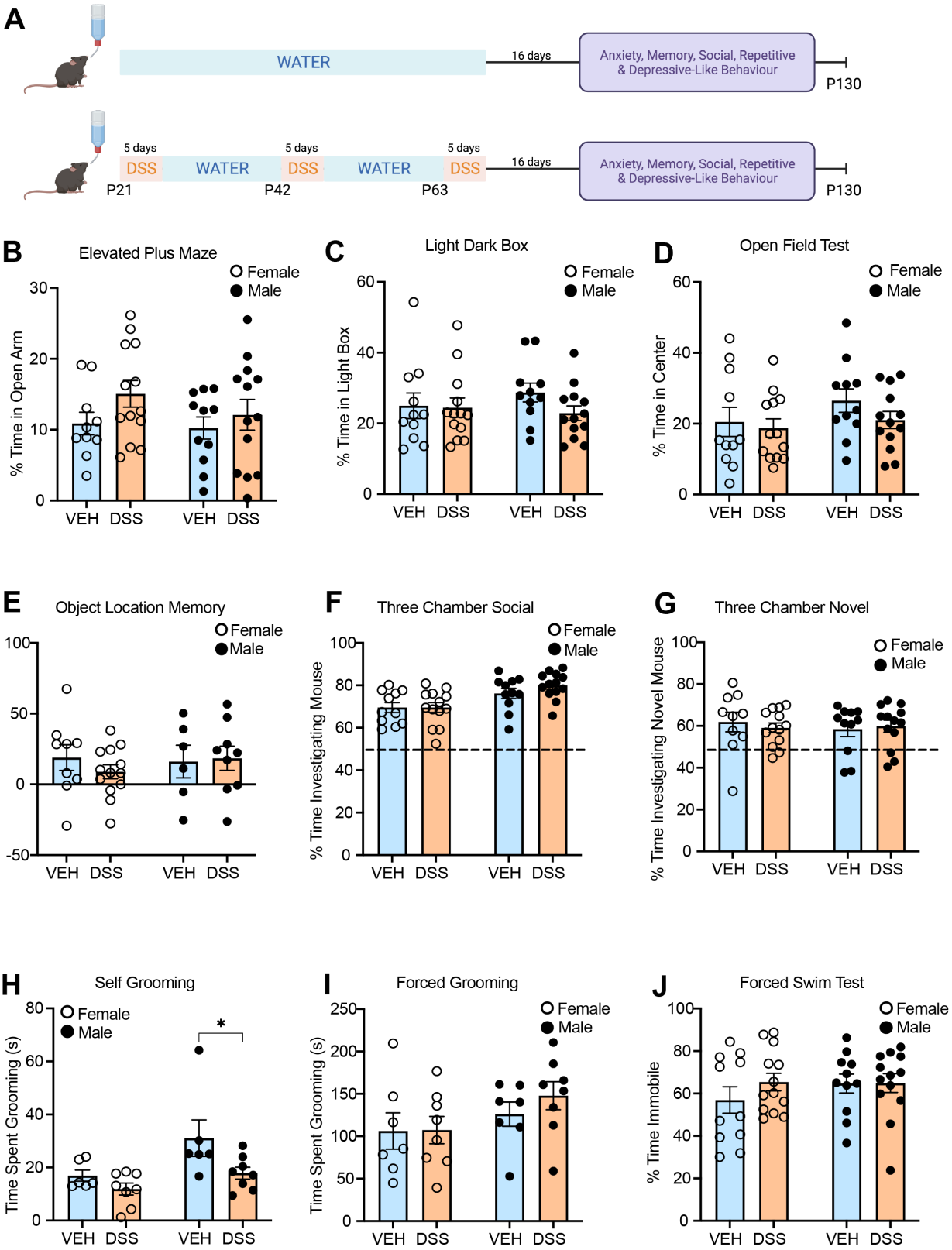
A
WATER
16 days
Anxiety, Memory, Social, Repetitive & Depressive-Like Behaviour
P130
5 days
DSS
WATER
DSS
WATER
DSS
P21
P42
P63
B
Elevated Plus Maze
% Time in Open Arm
C
Light Dark Box
% Time in Light Box
D
Open Field Test
% Time in Center
E
Object Location Memory
Discrimination Index
F
Three Chamber Social
% Time Investigating Mouse
G
Three Chamber Novel
% Time Investigating Novel Mouse
H
Self Grooming
Time Spent Grooming (s)
I
Forced Grooming
Time Spent Grooming (s)
J
Forced Swim Test
% Time Immobile
Female
Male
VEH
DSS

Figure 2. Early life DSS-inflammation has minimal impact on adult anxiety, social, memory, and depression-like behaviors. *A*. Experimental design. After a 16-day recovery period, a behavioral battery compared VEH and DSS treated mice on *B.* the elevated plus maze *C.* the light dark box *D.* the open field test *E*. the object location memory test (24hr) *F*. the three-chamber social task *G.* the three-chamber novel social task *H.* self-grooming *I*. forced grooming and *J.* the forced swim test. All graph bars and error bars represent the mean ± SEM. *$p<0.05$

Early-life DSS disrupts male preference for female odor

In human patients with IBD (Ballinger et al., 2003) and in mouse models, early-life inflammation delays puberty and sexual development (DeBoer et al., 2010; Deboer and Li, 2011). To test the impact of repeated bouts of inflammation on sexual behaviors in our model, ~1 month following DSS, mice were given a preference test for same- or opposite-sex urine (Figure 3A). Female VEH- and DSS-treated mice both failed to show a significant preference for either same-sex urine (VEH one sample t-test vs 50% $t(6) = 0.383$, $p=.714$ or DSS one sample t-test vs 50% $t(6) = 0.406$, $p=.70$) or opposite-sex urine (VEH one sample t-test vs 50% $t(6) = 0.350$, $p=0.74$ or one sample t-test vs 50% DSS $t(6) = 0.256$, $p=.81$) compared to water (Figure 3B). In contrast, male VEH-treated mice showed a significant preference for same-sex urine compared to water (one sample t-test vs 50% $t(7) = 2.468$, $p=.04$) and a trend for a preference for opposite-sex urine $t(7) = 1.972$, $p=.086$. However, male DSS-treated mice failed to show a preference for same-sex urine ($t(7) = 1.153$, $p=.29$) as well as opposite-sex urine over water ($t(7) = 0.99$, $p=.36$) (Figure 3C). When comparing preferences directly, there was no significant difference in VEH-treated and DSS-treated males in their preference for male urine ($t(14) = 1.45$, $p = .17$).

However, VEH-treated males showed a significantly higher preference for female urine than DSS-treated males ($t(14) = 2.16$, $p = .048$) (Figure 3C). Together, this demonstrates that DSS treatment produced a significant deficit in opposite-sex scent-seeking behaviors, a key aspect of mate-seeking behavior in male rodents (Malkesman et al., 2010).

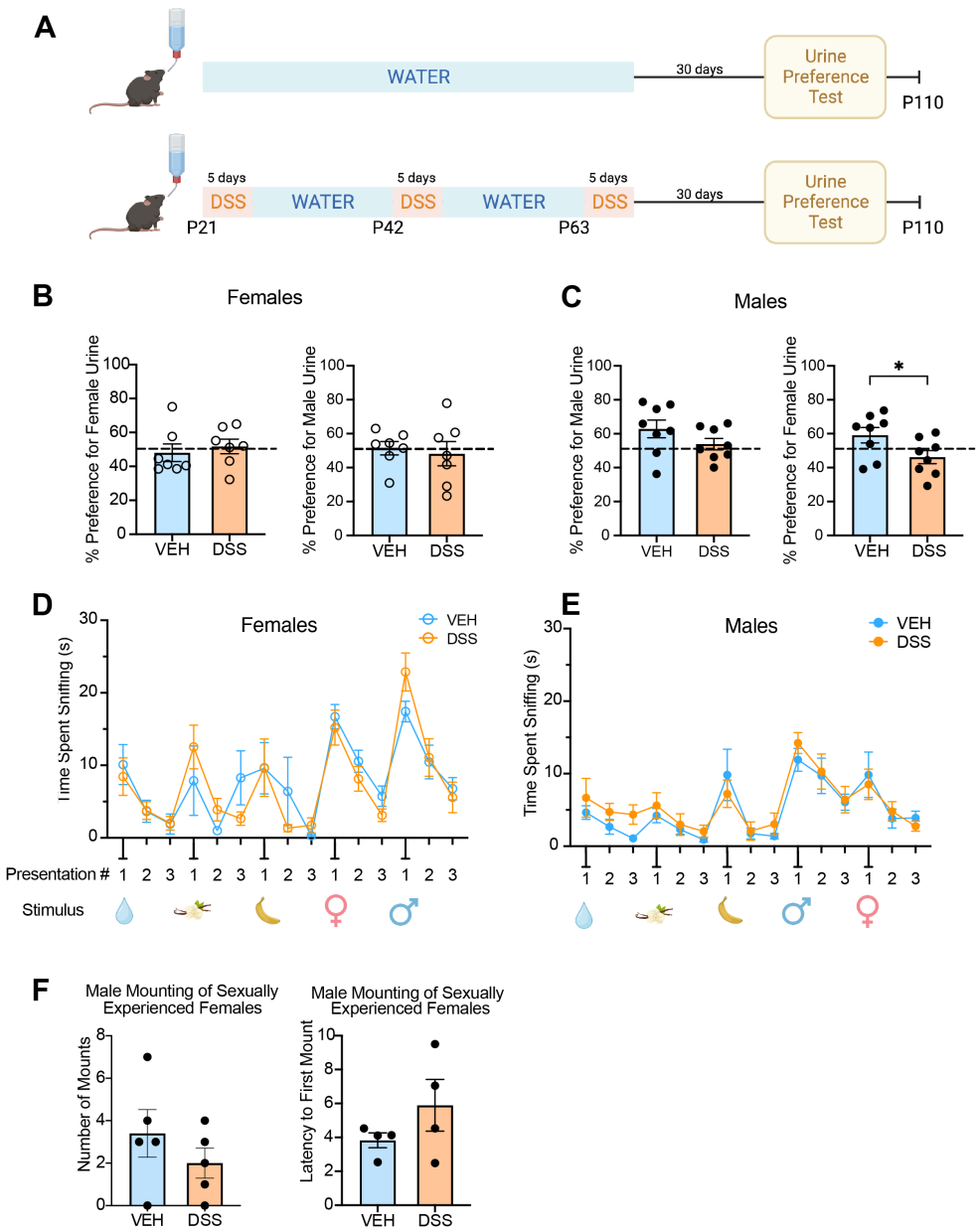

Figure 3. Early life DSS-inflammation induces male sex-specific impairments in mate-seeking behavior. *A*. Experimental design. After a 30-day recovery period mate seeking behavior was assessed by the Urine Preference Test. *B*. Female mice showed no preference for female or male urine over water and VEH and DSS mice perform similarly. Each graph bar and error bar represent the mean ± SEM. Dotted line is 50% preference. *C*. Male VEH mice significantly preferred both male and female urine over water (above 50% dotted line). DSS treated males showed no preference for urine over water. *D, E.* Olfactory habituation-dishabituation test for females (*D*) and males (*E*) revealed no differences between DSS- and VEH- treated mice and normal exploration, habituation and then dishabituation patterns for each odor. *F*. DSS and VEH male mice showed similar number of mounts and latency to first mount a sexually experienced female. *$p<0.05$.

To verify that deficits in the urine preference test in DSS-treated males were not due to impairments in olfaction, we performed the olfaction habituation-dishabituation task in which novel odors are presented to a mouse, which then habituates its exploration in response to repeated presentations (Yang and Crawley, 2009). When a new odor is then introduced, mice resume high levels of exploration and then habituate (Yang and Crawley, 2009). We tested two extract odors (vanilla and banana) and two social odors (one same sex and one opposite sex novel mouse odors). Both treatment groups and sexes showed the expected patterns of active exploration of each odor followed by habituation across repeated trials and then active exploration of the next novel odor (dishabituation) (Figure 3D and E and supplemental Table 1), indicating that DSS treatment did not negatively impact odor processing or recognition. Together, these findings demonstrate a long-term shift in male-specific preferences for female odors following early-life gut inflammation.

To further explore impacts on consummatory mating behaviors, we compared sexually naïve mounting behavior of the VEH- and DSS-treated male mice when paired with a sexually experienced untreated female wildtype control mouse. Over a 15-minute mating session, DSS-treated male mice showed no significant differences in copulatory behaviors compared to VEH males including frequency of mounting ($t(8) = 1.06$, $p = .32$) and latency to first mount ($t(6) = 1.30$, $p = .42$) (Figure 3F). Together, this suggests that early-life DSS treatment has specific deficits on mate-seeking through olfactory cues and not on consummatory sexual behavior.

Early-life intestinal inflammation disrupts androgens in males

Given the observed differences in urine odor preferences, we investigated reproductive organ development. Male and female reproductive organs were collected following behavior testing and weighed (P110). In males, there was a significant decrease in the weight of the androgen-sensitive seminal vesicles in the DSS-treated animals compared to VEH ($t(23) = 2.44$, $p =.03$) (Figure 4A). However, there was no significant difference in testes weight between treatments ($t(23) = 1.05$, $p = .30$) (Figure 4B). In females, we observed no difference in estrogen-sensitive uterus weight ($t(23) = 0.42$, $p = .68$) (Figure 4C). To further investigate the impairment in male seminal vesicle development, we examined changes in circulating steroid hormones in VEH- and DSS-treated male mice both acutely (P71, 3 days after final DSS treatment) (Figure 4D, E) and chronically (after behavioral testing, P110) (Figure 4F, G). At the acute timepoint (P71), the DSS-treated males showed a significant decrease in serum testosterone ($U = 0$, $p = 0.03$) and androstenedione ($U = 0$, $p = 0.03$) levels. This decrease was maintained through behavioral testing for androstenedione ($U = 27$, $p = 0.01$) but not for testosterone ($U = 46$, $p = 0.22$). There

were no significant differences in serum progesterone in males at either timepoint and no impacts in females for androstenedione, testosterone, or progesterone (Supplemental Figure 1). All together, these data indicate that early-life DSS treatment reduces male reproductive organs, potentially through reduced levels of circulating androgens.

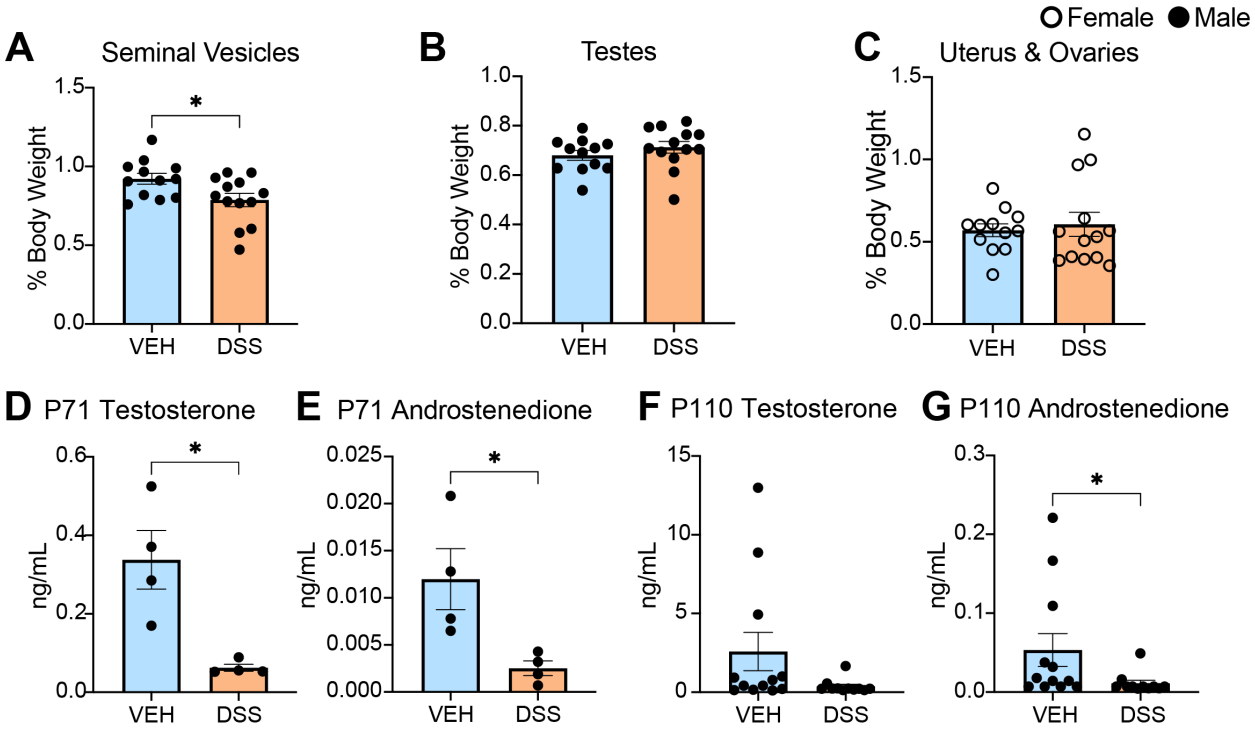

Figure 4. DSS induces male sex-specific impairments in reproductive physiology. *A*. Seminal vesicles were significantly lower in weight in DSS-treated male mice than VEH-treated mice at P110. *B*. There were no significant differences in testes weight between DSS- and VEH-treated males at P110. *C*. No significant differences in uterus and ovaries weights between DSS- and VEH-treated females were observed at P110. *D-E*. 3 days after the last DSS treatment (P71), male serum Testosterone (*D)* and Androstenedione (*E*) levels were significantly lower in DSS- than in VEH-treated mice. Each graph bar and error bar represent the mean ± SEM. *F-G*. Following the last behavioral experiment (P110), male plasma Testosterone (*D)* levels were not

significantly different between VEH and DSS mice, but Androstenedione (*E*) levels were significantly lower in DSS- than in VEH-treated mice. Each graph bar and error bar represent the mean ± SEM. *$p<0.05$.

Early-life intestinal inflammation alters SCFA/MCFA production and gut microbiome composition to favour decreased abundance of SCFA/MCFA-producing taxa

We then examined circulating short and medium-chain fatty acids (Figure 5A), which are produced by the gut microbiota, disrupted in IBD patients, and can alter sex steroids (Acharya et al., 2024). Acutely following the last round of DSS (P71), DSS treatment significantly reduced female ($p = 0.014$) and male ($p = 0.037$) serum levels of valeric acid (see Supplemental Table 1 for full statistics). In females, DSS also decreased serum levels of capric acid ($p = 0.022$) (Figure 5A). We also measured SCFA/MCFA levels in cecal contents. In the cecal contents, butyric acid was the only SCFA that was significantly different between VEH- and DSS-treated males ($p = 0.0498$) (Figure 5B, see Supplemental Table 1 for full statistics).

We then investigated whether SCFA-producing bacteria were differentially present in VEH- and DSS-treated mice acutely following the last round of DSS at P71 (Figure 5C, D). Differential abundance analysis revealed that DSS-treated female mice possessed decreased relative abundance of the phylum Bacillota ($p_{females} = 0.0130$), which contains many SCFA-producing bacterial species (Fusco et al., 2023; Mandal et al., 2015). Indeed, the relative abundance of Bacillota was moderately correlated with cecal acetic ($R = 0.54$, $p = 0.005$) and butyric acid ($R = 0.76$, $p < 0.001$) levels (Supplemental Figure 2A). Specifically, DSS-treated mice possessed decreased relative abundance of the families Lachnospiraceae ($p_{females} = 0.0102$, $p_{males} = 0.0222$)

and Lactobacillaceae ($p_{females}$ = 0.0136, p_{males} = 0.0173), and the genera *Roseburia* ($p_{females}$ = 0.0021, p_{males} = 0.0418), *Ruminococcus* ($p_{females}$ = 0.0107, p_{males} = 0.0075), along with several *Eubacterium* groups ([*Eubacterium*] ventriosum group, $p_{females}$ = 0.0063, p_{males} = 0.0202; [*Eubacterium*] xylanophilum group, $p_{females}$ = 0.0056, p_{males} = 0.0203; [*Eubacterium*] coprostanoligenes group, $p_{females}$ = 0.0138, p_{males} = 0.0054) – bacterial taxa that are known to produce SCFAs (Figure 5C, D, Supplemental Figure 2A) (Akhtar et al., 2021; Fusco et al., 2023; Mirzaei et al., 2021; Ziętek et al., 2021).

Of these differentially abundant taxa, many express β-glucuronidases and β-glucosidases, enzymes that convert conjugated hormones to their active form (Ervin et al., 2019; Patel et al., 2023). Strikingly, the relative abundance of several GUS-producing taxa was correlated with serum testosterone and androstenedioine concentrations (Figure 5E). For instance, the relative abundance of [*Eubacterium*] *ventriosum* group was positively correlated with circulating androstenedione (Spearman's correlation, R = 0.76, p = 0.03) and testosterone (R = 0.81, p = 0.016). Similarly, relative abundance of [*Eubacterium*] *coprostanoligenes* group was positively correlated with androgen levels (androstenedione, R = 0.91, p = 0.002; testosterone, R = 0.91, p = 0.002). Relative abundance of *Lactobacillus*, a member of the Lactobacillaceae family, was also positively correlated with serum androstenedione (R = 0.81, p = 0.022) and testosterone (R = 0.90, p = 0.005). In contrast, the relative abundance of *Bacteroides thetaiotaomicron*, which expresses a sulfotransferase that deactivate hormones (Cotton et al., 2023), was negatively correlated with testosterone concentrations (R = -0.74, p = 0.046) (Supplemental Figure 2B). Taken together, these findings indicate that early life inflammation alters microbiome composition, which correlates with androgen and SCFA levels.

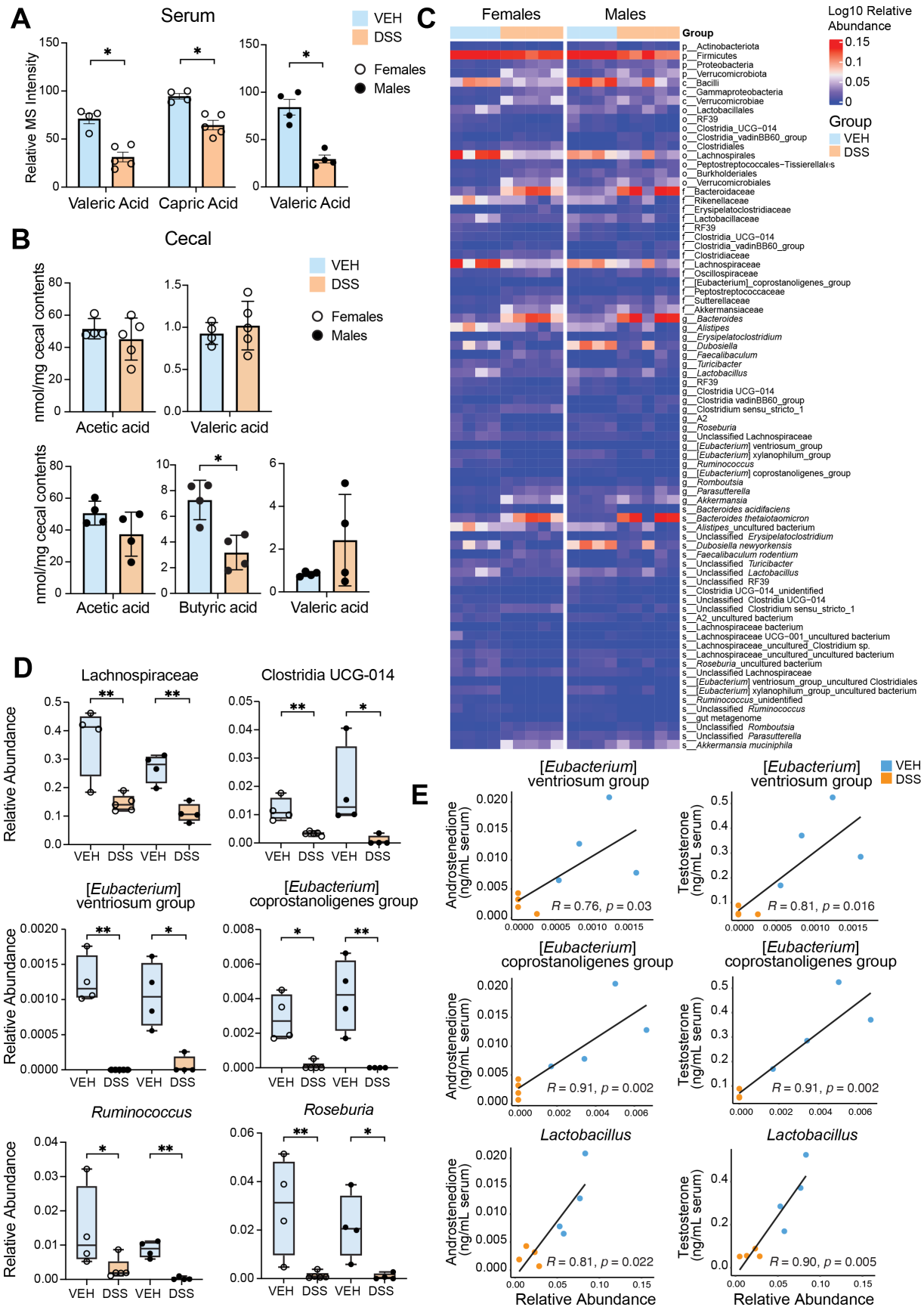
A
Serum
VEH
DSS
Females
Males
Relative MS Intensity
Valeric Acid
Capric Acid
Valeric Acid
B
Cecal
nmol/mg cecal contents
Acetic acid
Valeric acid
Butyric acid
C
Females
Males
Log10 Relative Abundance
Group
D
Lachnospiraceae
Clostridia UCG-014
[Eubacterium] ventriosum group
[Eubacterium] coprostanoligenes group
Ruminococcus
Roseburia
Relative Abundance
E
Androstenedione (ng/mL serum)
Testosterone (ng/mL serum)
R = 0.76, p = 0.03
R = 0.81, p = 0.016
R = 0.91, p = 0.002
R = 0.91, p = 0.002
R = 0.81, p = 0.022
R = 0.90, p = 0.005
Relative Abundance

Figure 5. Early life DSS-inflammation causes decreases in short- and medium-chain fatty acid levels and relative abundance of associated microbiota. *A*. Serum levels of valeric and caproic acid were significantly lower in DSS-treated females compared to VEH at P71. Valeric acid was also significantly lower in DSS-treated male serum. See Supplement for full set of serum statistics. *B.* Cecal levels SCFAs at P71, represented in nmol/mg of contents. Concentration of butyric acid was significantly different in DSS-treated males compared to VEH at P71. See Supplement for full set of cecal SCFA statistics. *C.* Heatmap of differentially abundant gut bacterial taxa identified by differential abundance testing at P71. *D.* Relative abundance boxplots of several SCFA-producing bacteria. *E.* Correlation of select SCFA-producing bacteria with serum testosterone and androstenedione concentrations. *$p<0.05$, **$p<0.01$.

Early life intestinal inflammation causes long-lasting physiological differences and changes to gut microbiota composition

We then investigated whether changes in microbial metabolites and abundance persisted into adulthood (P110). We first examined microbiome diversity as an indicator of overall lasting effect of DSS. At P110, the number of observed microbiota features remained significantly decreased in female DSS-treated mice compared to VEH ($p = 0.0207$) (Figure 6A). Additionally, although microbiota compositions (as calculated using Bray-Curtis distances) became more similar between DSS-treated and VEH mice, differences in sex and treatment remained significant (PERMANOVA, $p_{sex} = 0.001$, $p_{treatment} = 0.004$) (Figure 6B). Consistent with these long-lasting microbiota changes, analysis of colon histology revealed that DSS-treated

colons at P110 retained several indicators of inflammation at sparsely found regions throughout the gut, specifically intestinal crypt hyperplasia and increased immune cell infiltration (representative images shown, Figure 6C). Nevertheless, the majority of the epithelium along the length of the colon appeared to have recovered after ~40 days post cessation of DSS.

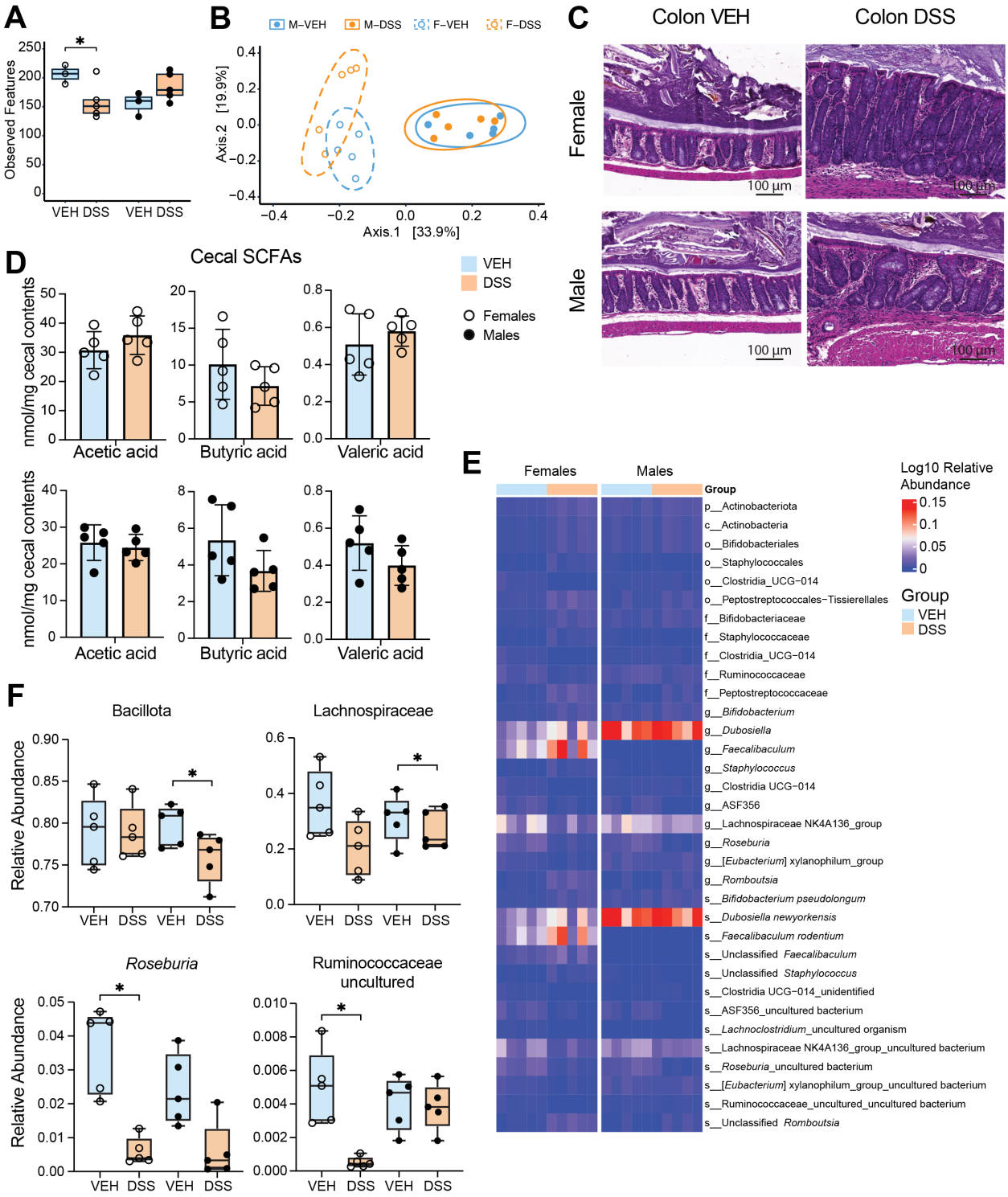

Figure 6. Early life inflammation causes long-lasting physiological differences and changes to microbiota composition. *A.* Diversity of microbiota composition ~30 days after cessation of

DSS at P110, measured in number of unique features per sample. *B.* Principal Component Analysis of Bray-Curtis diversity index at P110 shows lack of separation by treatment. *C.* Representative histological images of hematoxylin and eosin-stained colons at P110. *D.* Cecal concentrations of SCFAs at P110. See Supplement for full set of cecal measurements. *E.* Heatmap of taxa identified as differentially abundant between DSS and VEH-treated animals at P110. *F.* Relative abundance boxplots of select SCFA-producing taxa. *$p<0.05$.

Following these observations, we next sought to examine whether the microbiome composition would eventually equilibrate, and if these long-lasting changes were mirrored in microbial signaling molecules. First, we found that there were no significant differences in cecal SCFA levels between VEH- and DSS-treated mice at P110 (post reproductive behavioral testing, cohort shown in Figure 3) (Figure 6D). We then examined the microbiome at this timepoint, and found that many of the differentially abundant SCFA-producing taxa identified at P71 were no longer significantly different between treatments at P110. In addition, there were fewer significantly different taxa identified at P110 (Figure 6E) compared to the P71 (Figure 5C) acute timepoint, indicating that the microbiome composition was shifting towards recovery. However, those few taxa that remained differentially abundant included several known SCFA-producing taxa, including the phylum Bacillota ($p_{males} = 0.0198$), the family Lachnospiraceae ($p_{males} = 0.0181$), and the genera *Roseburia* ($p_{females} = 0.0476$) and an uncultured *Ruminococcaceae* ($p_{females} = 0.0157$) (Figure 6F). Overall, these persisting microbiota changes did not appear to correlate with serum hormone levels (Supplemental Table 1). Ultimately, these findings suggest that early life inflammation causes acute changes to the microbiome and microbial signaling molecules, the majority of which equilibrate in absence of further inflammation in adulthood.

Early-life intestinal inflammation disrupts microglial morphology and brain connectivity in both sexes

Microglia are sensitive to microbiota-derived metabolites and SCFAs specifically have been shown to alter microglial morphology and function during development (Erny et al., 2015). We therefore examined changes in microglial activation state in several brain regions following behavior at P110. Using our newly developed microglial morphology analysis tool (Kim, Jennifer et al., 2023), we measured 27 morphological features from 8,349 microglia in the dorsal hippocampus (average of 417 per mouse) (Figure 7), 5,971 microglia in the hypothalamus (average of 426 per mouse) and 8,482 microglia in the cortex (average of 446 per mouse) (Supplemental Figure 3).We identified four clusters of different morphologies (Figure 7A, Supplemental Figure 3D) including microglia showing ameboid, ramified, rod-like and hypertrophic characteristics. Within the dorsal hippocampus there was a significant treatment by cluster interaction for both sexes (Supplemental Table 1). Sidak corrected posthoc tests identified a significant decrease in ramified microglia and a trend towards an increase in ameboid microglia specifically in DSS-treated females (Figure 7B and C). In males there was a trend ($p=0.06$) towards an increase in hypertrophic microglia in the DSS-treated males. There were no significant differences in hypothalamic or cortical microglia between treatments in either sex (Supplemental Figure 3E-F). These differences in microglial morphology observed months after the early life DSS treatment indicate long-term reprogramming of microglial function.

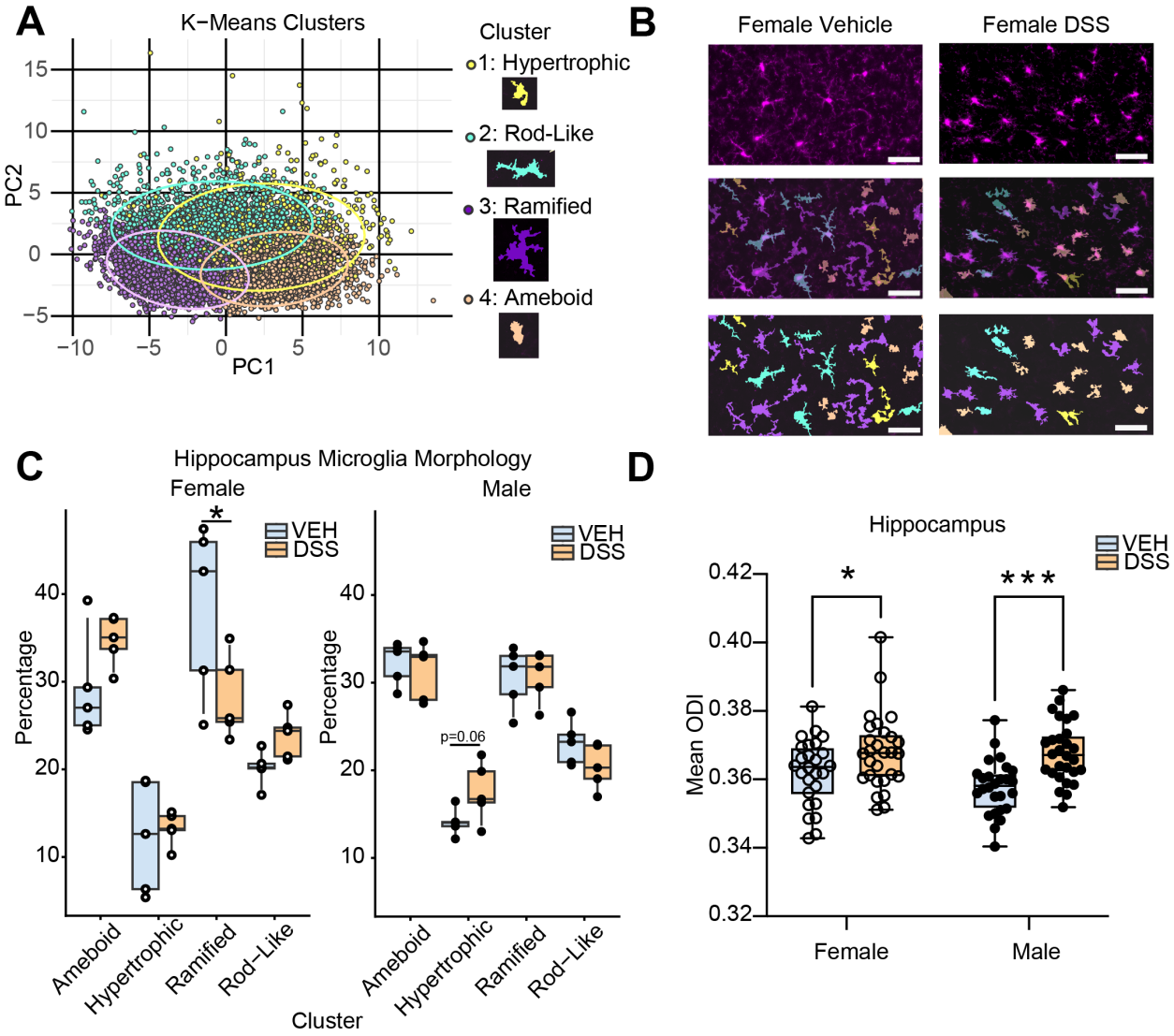

Figure 7. Long-Term Microglial Morphology and Brain Connectivity Changes Following Early Life DSS. *A*. K-means clustering of the the first three principal components from 27 individual microglial morphology metrics. Cluster optimization (Supplemental Figure 3B). revealed 4 clusters. Clusters were then assigned to morphology descriptions based on relationship to individual metrics. *B*. Example images from female vehicle and DSS treated dorsal hippocampus demonstrate changes in microglial morphology (P110). Top panel is Iba1 staining. Middle panel is the overlay with individual cell morphology clusters identified in A and the bottom panel is the individual cell labs for each cluster. All scale bars are 50 µm. *C.*

Quantification of the percentage of microglia within each cluster between treatment conditions for females and males. DSS significantly decreased the proportion of ramified microglia and trended towards an increase in ameboid microglia. A trend toward an increase in hypertrophic microglia was oberved in males *D.* Orientation dispersion index (ODI) was calculated for the bilateral hippocampus across all samples. Data points are mean ODI values from each sample. Both males and females had significant increases in ODI in the DSS treatment when compared to treatment with the vehicle alone. * = $p < 0.05$, *** = $p < 0.001$.

Clinical-translational quantitative neuroimaging reveals extraneuritic hippocampal microstructural changes following early life inflammation in both sexes

We performed ex-vivo multicompartment (MC) diffusion MRI and fit it to the neurite orientation and dispersion index (NODDI) model to assess and compare microstructural changes across biologically relevant regions (hippocampus, amygdala, striatum, thalamus, hypothalamus, frontal association cortex) between the VEH- and DSS-treated mice. MC diffusion MRI enables non-invasive characterization of neuronal cytoarchitecture at the mesoscale (1- 100µm). The NODDI model is particularly used to calculate the diffusion signal specific to intra-neurite and extra-neurite compartments of the brain and has previously been shown to have sensitivity to various neuropathological states (Barnett et al., 2019; Singh et al., 2023; Stowe et al., 2024; Yi et al., 2022). Specifically, the mean orientation dispersion index (ODI, extraneurite) and mean neurite density index (NDI, intraneurite) values were tested using a 2x2 ANOVA considering the effects of treatment and sex. For ODI, a significant main effect of treatment was identified in the hippocampus (FDR-adjusted $p = 0.0002$, partial $\eta^2 = 0.1560$) (Figure 7D). Post-hoc testing

identified that both males and females had a significant increase in their ODI value when treated with DSS compared to VEH (males: Fisher's LSD $p = 0.0001$; females: Fisher's LSD $p = 0.0269$). Additionally, a significant main effect of treatment was found in the thalamus (FDR-adjusted $p = 0.0095$, partial $\eta^2 = 0.0822$) (Supplemental Figure 4). Post-hoc testing indicated that females had a significant increase in their ODI value when treated with DSS compared to VEH, but that the increase in males did not reach significance (males: Fisher's LSD $p = 0.2353$; females: Fisher's LSD $p = 0.0023$). No significant treatment by sex interactions were identified in either the thalamus or hippocampus. No significant treatment or treatment by sex interaction effects were found in the frontal association cortex, amygdala, striatum, and hypothalamus. Furthermore, for NDI, no significant effects were identified in any of the regions of interest. Supplemental Table 1 contains the full findings for all regions tested. The significant differences in the ODI signal measured in our pediatric IBD model are consistent with the documented changes in microglial morphology, as we have seen in our previous work (Yi et al., 2019). Further, consistent with our cellular morphological studies, no significant changes were identified in the hypothalamus or cortex using NODDI.

Discussion

The incidence of IBD is high and increasing, especially in early life (Benchimol et al., 2017, 2014; Ng et al., 2017). IBD is particularly challenging when it develops in children; delay in the onset and progression through puberty is common in this population, and can result in reduced adult height and sexual immaturity (Gupta et al., 2020). In this study, we assessed the microbiome, intestinal, endocrine, brain, and behavioral effects of repeated DSS-induced gut

inflammation in early life. While early life gut inflammation did not impair the majority of the adult rodent behavioral repertoire, we identified a unique deficit in preference for female urine in DSS-treated male mice. These deficits in mate-seeking behavior corresponded to a decrease in seminal vesicle size, blunted circulating levels of androgen hormones and SCFAs, an altered gut microbiota and inflamed intestines. Microglia were altered in the hippocampus, indicating hippocampal dysfunction may contribute to reproductive behavioral deficits in males (Kight and McCarthy, 2020).

In our model, DSS significantly decreased seminal vesicle weight, circulating sex hormone levels, and impaired male-specific preference for female urine – a key aspect of mate-seeking behavior in rodents (Keller et al., 2008; Malkesman et al., 2010). These differences were not driven by impaired olfactory discrimination, as both sexes and treatments performed normally on the olfactory habituation-dishabituation paradigm. In both adolescent males and females with IBD, puberty onset is often and progression through puberty is often prolonged, especially in patients with disease relapses (Hildebrand et al., 1994). Adults with IBD report increased rates of sexual dysfunction (Bel et al., 2015), and infertility in both men (Hammami and Mahadevan, 2020) and women (Zhang et al., 2021; Zhao et al., 2019). This is consistent with findings from our study, where we found that DSS-treated male mice had decreased androgen hormones that may have directly contributed to the decrease in seminal vesicle weight (Yamane et al., 1986). Additionally, we observed that seminal vesicles in DSS-treated male mice were often not descended fully within the abdominal cavity. While we did not observe direct impacts on male mounting behavior, future work will be required to fully examine the impacts of early life DSS on adult male reproduction and fertility.

Research suggests that hormone supplementation could potentially alleviate symptoms of IBD (Nasser et al., 2015; Rosen et al., 2015). However, the use of hormone supplementation in adolescents with IBD is contentious and can pose substantial risks due to potential side effects such as weight gain, mood changes, sleep disruption, and increased susceptibility to infections (Bishop et al., 2014). This necessitates new, non-hormone based therapies for treating adolescent IBD. The microbiota represents a potential lever for management of IBD-mediated alterations in hormones and development. Germ-free mice are known to have changes in sex hormones and pubertal onset (Markle et al., 2013; Weger et al., 2019), suggesting that the gut microbiome regulates sex hormone levels of the host. Furthermore, sex hormones can in turn regulate the gut microbiome. This bidirectional relationship develops during puberty (Korpela et al., 2021). In both sexes, puberty is marked by increasing abundance of estrogen-metabolizing Clostridia and decreasing abundance of Bacteroidia (Korpela et al., 2021). Specific gut microbiota members secrete β-glucuronidase and β-glucosidase enzymes that deconjugate estrogens and androgens back to their active form (Ervin et al., 2019; Patel et al., 2023). These re-activated hormones are then secreted back into the circulating blood, where they can act throughout the body. In humans, estrogen levels are strongly and significantly associated with fecal Clostridia taxa, including three genera in the Ruminococcaceae family (Flores et al., 2012). This suggests that gut microbial families such as Ruminococcaceae may directly influence levels of host sex-hormones such as estrogen. Disruption of β-glucuronidase-producing microbiota results in a reduction in circulating estrogens (Baker et al., 2017), impairing the feedback loop between sex hormone levels and gut microbiota composition. In our novel model of pediatric IBD, we report differences in the key β-glucuronidase-expressing genus *Roseburia* acutely following the final round of DSS treatment, along with several *Eubacterium* groups that are known to deconjugate

estrogens (Ervin et al., 2019). The relative abundance of these taxa were positively correlated with serum testosterone and androstenedione concentrations, highlighting the potential involvement of these gut microbes in regulating systemic hormone levels. Together, this suggests that future microbiota-targeted therapeutics specifically impacting hormone regulating microbes could potentially offset the negative effects of IBD on sexual health.

How changes in gut inflammation drive endocrine, brain and behavior changes is not well understood, but metabolite signalling molecules have been proposed as a potential link between all three systems (Silva et al., 2020). A number of metabolites have been implicated in IBD pathogenesis, including SCFAs, secondary bile acids (SBA) and tryptophan (Lavelle and Sokol, 2020; Sinha et al., 2020). Microglia have receptors for short-chain fatty acids (SCFA) (Erny et al., 2015) and secondary bile acids (SBA), both which are produced by gut microbiota and are reduced in IBD patients (Lavelle and Sokol, 2020). These microbiota-derived metabolic signals can cross the blood-brain barrier (Mertens et al., 2017; Mitchell et al., 2011; Wenzel et al., 2020) and are critical for normal microglial development and function (Erny et al., 2015; Thion et al., 2017). In our study, we found more differences in SCFA/MCFA abundances in DSS mice in the serum compared to within the cecal contents. This difference could be due to SCFAs being absorbed by host cells for use as energy sources. In particular, intestinal epithelial cells utilize SCFAs (particularly butyric acid) as a main source of energy, causing the concentration of SCFAs in the blood to decrease compared to what is measured in the cecum (den Besten et al., 2013). It has also been shown that butyrate uptake by colonocytes is impaired in inflamed IBD patient tissues (Thibault et al., 2010). Thus, DSS-induced inflammation could cause decoupling of cecal and serum SCFA concentrations. The reduced levels of SCFAs observed in our pediatric IBD model may be responsible for the abnormal microglial morphology we observed, with

potential negative impacts on microglial regulation of neural circuit formation during formative years in childhood and adolescence. Importantly, as we gain deeper insight into the causal mechanisms underpinning abnormal microglial function in pediatric IBD, the potential for innovative clinical interventions to abrogate these deleterious effects become possible. In order to test the therapeutic efficacy of any future intervention, diagnostic biomarkers and biomarkers of therapeutic response are critically needed. Herein, we demonstrated the sensitivity of NODDI quantitative diffusion imaging to alterations in microglial morphology and moreover, demonstrate both the sensitivity of NODDI to changes in the hippocampus as well as its specificity to the absence of significant changes in the thalamus, hypothalamus, and cortex. Further, consistent with our prior work (Yi et al., 2019), these changes in microglial morphology were detected in the ODI signal alone, demonstrating the sensitivity of the ODI signal to alterations in microglia.

Finally, our main behavioral battery tested mouse anxiolytic, repetitive, cognitive, social and depressive-like behavior and found no significant differences between control and DSS-treated mice. This is in contrast to previous findings (Salvo et al., 2020), where 5 days of DSS at weaning (P21) resulted in behavioral deficits on the novel object recognition task and light-dark task in adulthood (P56). Several study design aspects differentiate this previous work from our current study that may explain why the same impacts were not found. Firstly, the current study modelled a more chronic IBD phenotype with 3 rounds of DSS treatments in early life. The chronic nature of the current study may have induced resiliency and a faster recovery than in a single DSS treatment. Salvo et al. also did not identify any sex differences in their model. In contrast, we have observed impacts specifically on male development and differential impacts of treatment in males and females on behavior, metabolites, brain connectivity and microglial

morphology. Future work is required to replicate and extend both sets of findings to identify how timing of DSS treatment impacts reproductive health (including the onset of puberty) as well as impacts on brain and behavioral development.

The incidence of pediatic onset IBD disease has doubled in the last 10 years (Ashton and Beattie, 2024), and young children with IBD often have more severe disease and more frequent health visits than adults (Benchimol et al., 2011). Their illness also imposes a large emotional and financial toll on families and caregivers (Herzer et al., 2011). Developing effective treatments for adolescents with IBD holds great promise, as reducing inflammation early in the disease course may prevent long-term complications, need for surgery, and hospitalization. Our novel mouse model of pediatric onset IBD, which captures alterations in the microbiome, microbial signaling molecules and brain-behavior disruptsion, represents a unique avenue for advancing our mechanistic understanding of IBD in this key subpopulation. Our findings open the door for new treatment avenues for therapeutics targeted to adolescents with IBD, with minimal side effects and maximal benefits for growth, development, and quality of life.

Funding

Research Corporation for Science Advancement, Scialog SA-MND-2021-001 (to CT, JPY). Canadian Institutes of Health Research (CIHR) Project Grant (to AVC, CT), Michael Smith Foundation Health Research Scholar Award (to CT, AVC), Canada Tier 2 Research Chair, Quantitative Microbiota Biology for Health Applications (to CT), Canada Tier 2 Research Chair, Understanding Gene Expression in the Brain (to AVC), Paul Allen Distinguished Investigator Award (to C.T.), Johnson & Johnson WiSTEM2D Award (to C.T.), Brain Canada

Future Leaders Award (to AVC), Research Corporation for Science Advancement Award (to AVC), UBC DMCBH pilot award (to AVC), National Sciences and Engineering Research Council of Canada (NSERC) Discovery Grant (RGPIN-2020-04895) (to TH), PEO International Peace Scholarship and World Universities Ramsay Postgraduate Scholarship (to SC). None of the funding sources influenced any aspect of the study design, data collection, analysis, interpretation or writing of the manuscript.

Available code and raw data

All supporting code for MicrogliaMorphology is available on Github at https://github.com/ciernialab/MicrogliaMorphology.

Acknowledgements

The authors acknowledge that the land we performed this research on is the traditional, ancestral, and unceded territory of the xwməθkwəy̓əm (Musqueam) Nation. The land it is situated on has always been a place of learning for the Musqueam people, who for millennia have passed on in their culture, history, and traditions from one generation to the next on this site. We encourage others to learn more about the native lands in which they live and work at https://native-land.ca/.

This work would not be possible without the help of numerous core facilities. In particular, the authors would like to acknowledge the staff at the Centre for Disease Modeling (CDM) at UBC, Ingrid Barta at UBC Animal Care Services (ACS) Histology, and the UBC Biofactorial High-Throughput Biology Facility, supported by the University of British Columbia Global Research

Excellence Biological Resilience Initiative. Thank you to the Djavad Mowafaghian Centre for Brain Health NeuroImaging and NeuroComputation Core (NINC) for data storage and computational resources. Additionally, we would like to thank the Kopp Lab at UBC for allowing use of their tissue processor, embedder, microtome, and slide scanner. Finally, this work received support from the BC Children's Hospital Histology Core, Dr. Andy Sham, Dr. Catherine Chan, and the team from the Gut4Health Microbiome Core Facility at the BC Children's Hospital Research Institute, Lisa Nikolai from the Chromatography Facility at the Faculty of Agricultural, Life & Environmental Sciences at the University of Alberta, and Dr. Ian Nation from Animal Pathology Services Ltd. (Canmore, Alberta). Thank you to Dr. Shelly McErlane for consultation on sex organ collection in mice. Thank you to the Centre for Disease Modeling staff and animal technicians for assistance with mouse experiments and animal care.

References

Acharya, A., Shetty, S.S., Kumari N, S., 2024. Role of gut microbiota derived short chain fatty acid metabolites in modulating female reproductive health. Human Nutrition & Metabolism 36, 200256. https://doi.org/10.1016/j.hnm.2024.200256

Akhtar, M., Chen, Y., Ma, Z., Zhang, X., Shi, D., Khan, J.A., Liu, H., 2021. Gut microbiota-derived short chain fatty acids are potential mediators in gut inflammation. Anim Nutr 8, 350–360. https://doi.org/10.1016/j.aninu.2021.11.005

Alatab, S., Sepanlou, S.G., Ikuta, K., Vahedi, H., Bisignano, C., Safiri, S., Sadeghi, A., Nixon, M.R., Abdoli, A., Abolhassani, H., Alipour, V., Almadi, M.A.H., Almasi-Hashiani, A., Anushiravani, A., Arabloo, J., Atique, S., Awasthi, A., Badawi, A., Baig, A.A.A., Bhala, N., Bijani, A., Biondi, A., Borzì, A.M., Burke, K.E., Carvalho, F., Daryani, A., Dubey,

M., Eftekhari, A., Fernandes, E., Fernandes, J.C., Fischer, F., Haj-Mirzaian, Arvin, Haj-Mirzaian, Arya, Hasanzadeh, A., Hashemian, M., Hay, S.I., Hoang, C.L., Househ, M., Ilesanmi, O.S., Balalami, N.J., James, S.L., Kengne, A.P., Malekzadeh, M.M., Merat, S., Meretoja, T.J., Mestrovic, T., Mirrakhimov, E.M., Mirzaei, H., Mohammad, K.A., Mokdad, A.H., Monasta, L., Negoi, I., Nguyen, T.H., Nguyen, C.T., Pourshams, A., Poustchi, H., Rabiee, M., Rabiee, N., Ramezanzadeh, K., Rawaf, D.L., Rawaf, S., Rezaei, N., Robinson, S.R., Ronfani, L., Saxena, S., Sepehrimanesh, M., Shaikh, M.A., Sharafi, Z., Sharif, M., Siabani, S., Sima, A.R., Singh, J.A., Soheili, A., Sotoudehmanesh, R., Suleria, H.A.R., Tesfay, B.E., Tran, B., Tsoi, D., Vacante, M., Wondmieneh, A.B., Zarghi, A., Zhang, Z.-J., Dirac, M., Malekzadeh, R., Naghavi, M., 2020. The global, regional, and national burden of inflammatory bowel disease in 195 countries and territories, 1990–2017: a systematic analysis for the Global Burden of Disease Study 2017. The Lancet Gastroenterology & Hepatology 5, 17–30. https://doi.org/10.1016/S2468-1253(19)30333-4

Alexander, D.C., Hubbard, P.L., Hall, M.G., Moore, E.A., Ptito, M., Parker, G.J.M., Dyrby, T.B., 2010. Orientationally invariant indices of axon diameter and density from diffusion MRI. Neuroimage 52, 1374–1389. https://doi.org/10.1016/j.neuroimage.2010.05.043

Amann, R.I., Binder, B.J., Olson, R.J., Chisholm, S.W., Devereux, R., Stahl, D.A., 1990. Combination of 16S rRNA-targeted oligonucleotide probes with flow cytometry for analyzing mixed microbial populations. Appl Environ Microbiol 56, 1919–1925. https://doi.org/10.1128/aem.56.6.1919-1925.1990

Ananthakrishnan, A.N., 2013. Environmental Risk Factors for Inflammatory Bowel Disease. Gastroenterol Hepatol (N Y) 9, 367–374.

Andrews, S., 2010. FastQC: A Quality Control tool for High Throughput Sequence Data [WWW Document]. FASTQC: A Quality Control tool for High Throughput Sequence Data. URL https://www.bioinformatics.babraham.ac.uk/projects/fastqc/ (accessed 5.15.24).

Arganda-Carreras, I., Fernández-González, R., Muñoz-Barrutia, A., Ortiz-De-Solorzano, C., 2010. 3D reconstruction of histological sections: Application to mammary gland tissue. Microscopy Research and Technique 73, 1019–1029. https://doi.org/10.1002/jemt.20829

Ashton, J.J., Beattie, R.M., 2024. Inflammatory bowel disease: recent developments. Arch Dis Child 109, 370–376. https://doi.org/10.1136/archdischild-2023-325668

Attree, E.A., Dancey, C.P., Keeling, D., Wilson, C., 2003. Cognitive Function in People With Chronic Illness: Inflammatory Bowel Disease and Irritable Bowel Syndrome. Applied Neuropsychology 10, 96–104. https://doi.org/10.1207/S15324826AN1002_05

Azooz, O.G., Farthing, M.J.G., Savage, M.O., Ballinger, A.B., 2001. Delayed puberty and response to testosterone in a rat model of colitis. American Journal of Physiology-Regulatory, Integrative and Comparative Physiology 281, R1483–R1491. https://doi.org/10.1152/ajpregu.2001.281.5.R1483

Baker, J.M., Al-Nakkash, L., Herbst-Kralovetz, M.M., 2017. Estrogen–gut microbiome axis: Physiological and clinical implications. Maturitas 103, 45–53. https://doi.org/10.1016/j.maturitas.2017.06.025

Ballinger, A.B., Savage, M.O., Sanderson, I.R., 2003. Delayed Puberty Associated with Inflammatory Bowel Disease. Pediatr Res 53, 205–210. https://doi.org/10.1203/01.PDR.0000047510.65483.C9

Banfi, D., Moro, E., Bosi, A., Bistoletti, M., Cerantola, S., Crema, F., Maggi, F., Giron, M.C., Giaroni, C., Baj, A., 2021. Impact of Microbial Metabolites on Microbiota–Gut–Brain

Axis in Inflammatory Bowel Disease. Int J Mol Sci 22, 1623. https://doi.org/10.3390/ijms22041623

Bao, C.H., Liu, P., Liu, H.R., Wu, L.Y., Shi, Y., Chen, W.F., Qin, W., Lu, Y., Zhang, J.Y., Jin, X.M., Wang, X.M., Zhao, J.M., Liu, X.M., Tian, J., Wu, H.G., 2015. Alterations in brain grey matter structures in patients with Crohn's disease and their correlation with psychological distress. Journal of Crohn's and Colitis. https://doi.org/10.1093/ecco-jcc/jjv057

Bayless, D.W., Davis, C.-H.O., Yang, R., Wei, Y., de Andrade Carvalho, V.M., Knoedler, J.R., Yang, T., Livingston, O., Lomvardas, A., Martins, G.J., Vicente, A.M., Ding, J.B., Luo, L., Shah, N.M., 2023. A neural circuit for male sexual behavior and reward. Cell 186, 3862-3881.e28. https://doi.org/10.1016/j.cell.2023.07.021

Bel, L.G.J., Vollebregt, A.M., Van der Meulen-de Jong, A.E., Fidder, H.H., Ten Hove, W.R., Vliet-Vlieland, C.W., Ter Kuile, M.M., de Groot, H.E., Both, S., 2015. Sexual Dysfunctions in Men and Women with Inflammatory Bowel Disease: The Influence of IBD-Related Clinical Factors and Depression on Sexual Function. J Sex Med 12, 1557–1567. https://doi.org/10.1111/jsm.12913

Benchimol, E.I., Bernstein, C.N., Bitton, A., Carroll, M.W., Singh, H., Otley, A.R., Vutcovici, M., El-Matary, W., Nguyen, G.C., Griffiths, A.M., Mack, D.R., Jacobson, K., Mojaverian, N., Tanyingoh, D., Cui, Y., Nugent, Z.J., Coulombe, J., Targownik, L.E., Jones, J.L., Leddin, D., Murthy, S.K., Kaplan, G.G., 2017. Trends in epidemiology of pediatric inflammatory bowel disease in Canada: Distributed network analysis of multiple population-based provincial health administrative databases. American Journal of Gastroenterology 112, 1120–1134. https://doi.org/10.1038/ajg.2017.97

Benchimol, E.I., Manuel, D.G., Guttmann, A., Nguyen, G.C., Mojaverian, N., Quach, P., Mack, D.R., 2014. Changing age demographics of inflammatory bowel disease in Ontario, Canada: A population-based cohort study of epidemiology trends. Inflammatory Bowel Diseases. https://doi.org/10.1097/MIB.0000000000000103

Benchimol, E.I., To, T., Griffiths, A.M., Rabeneck, L., Guttmann, A., 2011. Outcomes of pediatric inflammatory bowel disease: Socioeconomic status disparity in a universal-access healthcare system. Journal of Pediatrics 158. https://doi.org/10.1016/j.jpeds.2010.11.039

Bercik, P., Park, A.J., Sinclair, D., Khoshdel, A., Lu, J., Huang, X., Deng, Y., Blennerhassett, P.A., Fahnestock, M., Moine, D., Berger, B., Huizinga, J.D., Kunze, W., McLean, P.G., Bergonzelli, G.E., Collins, S.M., Verdu, E.F., 2011. The anxiolytic effect of Bifidobacterium longum NCC3001 involves vagal pathways for gut–brain communication. Neurogastroenterology & Motility 23, 1132–1139. https://doi.org/10.1111/j.1365-2982.2011.01796.x

Bishop, J., Lemberg, D., Day, A., 2014. Managing inflammatory bowel disease in adolescent patients. Adolesc Health Med Ther 5, 1–13. https://doi.org/10.2147/AHMT.S37956

Bolyen, E., Rideout, J.R., Dillon, M.R., Bokulich, N.A., Abnet, C.C., Al-Ghalith, G.A., Alexander, H., Alm, E.J., Arumugam, M., Asnicar, F., Bai, Y., Bisanz, J.E., Bittinger, K., Brejnrod, A., Brislawn, C.J., Brown, C.T., Callahan, B.J., Caraballo-Rodríguez, A.M., Chase, J., Cope, E.K., Da Silva, R., Diener, C., Dorrestein, P.C., Douglas, G.M., Durall, D.M., Duvallet, C., Edwardson, C.F., Ernst, M., Estaki, M., Fouquier, J., Gauglitz, J.M., Gibbons, S.M., Gibson, D.L., Gonzalez, A., Gorlick, K., Guo, J., Hillmann, B., Holmes, S., Holste, H., Huttenhower, C., Huttley, G.A., Janssen, S., Jarmusch, A.K., Jiang, L.,

Kaehler, B.D., Kang, K.B., Keefe, C.R., Keim, P., Kelley, S.T., Knights, D., Koester, I., Kosciolek, T., Kreps, J., Langille, M.G.I., Lee, J., Ley, R., Liu, Y.-X., Loftfield, E., Lozupone, C., Maher, M., Marotz, C., Martin, B.D., McDonald, D., McIver, L.J., Melnik, A.V., Metcalf, J.L., Morgan, S.C., Morton, J.T., Naimey, A.T., Navas-Molina, J.A., Nothias, L.F., Orchanian, S.B., Pearson, T., Peoples, S.L., Petras, D., Preuss, M.L., Pruesse, E., Rasmussen, L.B., Rivers, A., Robeson, M.S., Rosenthal, P., Segata, N., Shaffer, M., Shiffer, A., Sinha, R., Song, S.J., Spear, J.R., Swafford, A.D., Thompson, L.R., Torres, P.J., Trinh, P., Tripathi, A., Turnbaugh, P.J., Ul-Hasan, S., van der Hooft, J.J.J., Vargas, F., Vázquez-Baeza, Y., Vogtmann, E., von Hippel, M., Walters, W., Wan, Y., Wang, M., Warren, J., Weber, K.C., Williamson, C.H.D., Willis, A.D., Xu, Z.Z., Zaneveld, J.R., Zhang, Y., Zhu, Q., Knight, R., Caporaso, J.G., 2019. Reproducible, interactive, scalable and extensible microbiome data science using QIIME 2. Nat Biotechnol 37, 852–857. https://doi.org/10.1038/s41587-019-0209-9

Brain, C.E., Savage, M.O., 1994. Growth and puberty in chronic inflammatory bowel disease. Baillieres Clin Gastroenterol 8, 83–100. https://doi.org/10.1016/s0950-3528(06)80020-5

Brooks, M.E., Kristensen, K., Benthem, K.J. van, Magnusson, A., Berg, C.W., Nielsen, A., Skaug, H.J., Mächler, M., Bolker, B.M., 2017. glmmTMB Balances Speed and Flexibility Among Packages for Zero-inflated Generalized Linear Mixed Modeling. The R Journal 9, 378–400.

Callahan, B.J., McMurdie, P.J., Rosen, M.J., Han, A.W., Johnson, A.J.A., Holmes, S.P., 2016. DADA2: High-resolution sample inference from Illumina amplicon data. Nat Methods 13, 581–583. https://doi.org/10.1038/nmeth.3869

Cao, Y., Dong, Q., Wang, D., Zhang, P., Liu, Y., Niu, C., 2022. microbiomeMarker: an R/Bioconductor package for microbiome marker identification and visualization. Bioinformatics 38, 4027–4029. https://doi.org/10.1093/bioinformatics/btac438

Chassaing, B., Aitken, J.D., Malleshappa, M., Vijay-Kumar, M., 2014. Dextran Sulfate Sodium (DSS)-Induced Colitis in Mice. Curr Protoc Immunol 104, Unit-15.25. https://doi.org/10.1002/0471142735.im1525s104

Chen, D., Zhou, C., Luo, Q., Chen, C., Liu, G., 2024. A Mendelian randomization study on causal effects of inflammatory bowel disease on the risk of erectile dysfunction. Sci Rep 14, 2137. https://doi.org/10.1038/s41598-024-52712-1

Colldén, H., Landin, A., Wallenius, V., Elebring, E., Fändriks, L., Nilsson, M.E., Ryberg, H., Poutanen, M., Sjögren, K., Vandenput, L., Ohlsson, C., 2019. The gut microbiota is a major regulator of androgen metabolism in intestinal contents. American Journal of Physiology-Endocrinology and Metabolism 317, E1182–E1192. https://doi.org/10.1152/ajpendo.00338.2019

Cotton, S., Clayton, C.A., Tropini, C., 2023. Microbial endocrinology: the mechanisms by which the microbiota influences host sex steroids. Trends in Microbiology 31, 1131–1142. https://doi.org/10.1016/j.tim.2023.03.010

Cryan, J.F., Dinan, T.G., 2012. Mind-altering microorganisms: The impact of the gut microbiota on brain and behaviour. Nature Reviews Neuroscience 13, 701–712. https://doi.org/10.1038/nrn3346

Däbritz, J., Gerner, P., Enninger, A., Claßen, M., Radke, M., 2017. Inflammatory Bowel Disease in Childhood and Adolescence. Dtsch Arztebl Int 114, 331–338. https://doi.org/10.3238/arztebl.2017.0331

De Wolfe, T.J., Wright, E.S., 2023. Multi-factorial examination of amplicon sequencing workflows from sample preparation to bioinformatic analysis. BMC Microbiol 23, 107. https://doi.org/10.1186/s12866-023-02851-8

Deboer, M.D., Li, Y., 2011. Puberty Is Delayed in Male Mice With Dextran Sodium Sulfate Colitis Out of Proportion to Changes in Food Intake, Body Weight, and Serum Levels of Leptin. Pediatr Res 69, 34–39. https://doi.org/10.1203/PDR.0b013e3181ffee6c

DeBoer, M.D., Li, Y., Cohn, S., 2010. Colitis causes delay in puberty in female mice out of proportion to changes in leptin and corticosterone. J Gastroenterol 45, 277–284. https://doi.org/10.1007/s00535-009-0192-x

den Besten, G., van Eunen, K., Groen, A.K., Venema, K., Reijngoud, D.-J., Bakker, B.M., 2013. The role of short-chain fatty acids in the interplay between diet, gut microbiota, and host energy metabolism. Journal of Lipid Research 54, 2325–2340. https://doi.org/10.1194/jlr.R036012

Dixon, P., 2003. VEGAN, a package of R functions for community ecology. Journal of Vegetation Science 14, 927–930. https://doi.org/10.1111/j.1654-1103.2003.tb02228.x

Eichele, D.D., Kharbanda, K.K., 2017. Dextran sodium sulfate colitis murine model: An indispensable tool for advancing our understanding of inflammatory bowel diseases pathogenesis. World J Gastroenterol 23, 6016–6029. https://doi.org/10.3748/wjg.v23.i33.6016

Emge, J.R., Huynh, K., Miller, E.N., Kaur, M., Reardon, C., Barrett, K.E., Gareau, M.G., 2016. Modulation of the microbiota-gut-brain axis by probiotics in a murine model of inflammatory bowel disease. American Journal of Physiology-Gastrointestinal and Liver Physiology 310, G989–G998. https://doi.org/10.1152/ajpgi.00086.2016

Erny, D., De Angelis, A.L.H., Jaitin, D., Wieghofer, P., Staszewski, O., David, E., Keren-Shaul, H., Mahlakoiv, T., Jakobshagen, K., Buch, T., Schwierzeck, V., Utermöhlen, O., Chun, E., Garrett, W.S., Mccoy, K.D., Diefenbach, A., Staeheli, P., Stecher, B., Amit, I., Prinz, M., 2015. Host microbiota constantly control maturation and function of microglia in the CNS. Nature Neuroscience 18, 965–977. https://doi.org/10.1038/nn.4030

Ervin, S.M., Li, H., Lim, L., Roberts, L.R., Liang, X., Mani, S., Redinbo, M.R., 2019. Gut microbial β-glucuronidases reactivate estrogens as components of the estrobolome that reactivate estrogens. Journal of Biological Chemistry 294, 18586–18599. https://doi.org/10.1074/jbc.RA119.010950

Flores, R., Shi, J., Fuhrman, B., Xu, X., Veenstra, T.D., Gail, M.H., Gajer, P., Ravel, J., Goedert, J.J., 2012. Fecal microbial determinants of fecal and systemic estrogens and estrogen metabolites: a cross-sectional study. Journal of Translational Medicine 10, 253. https://doi.org/10.1186/1479-5876-10-253

Fusco, W., Lorenzo, M.B., Cintoni, M., Porcari, S., Rinninella, E., Kaitsas, F., Lener, E., Mele, M.C., Gasbarrini, A., Collado, M.C., Cammarota, G., Ianiro, G., 2023. Short-Chain Fatty-Acid-Producing Bacteria: Key Components of the Human Gut Microbiota. Nutrients 15, 2211. https://doi.org/10.3390/nu15092211

Gaidos, J.K.J., Naik, K., Dave, J., Yao, M., Hou, J.K., Cipher, D.J., Smith, A.D., Feagins, L.A., 2020. High Prevalence of Male Sexual Dysfunction in a Prospective Multicenter VA Inflammatory Bowel Disease Population. Crohns Colitis 360 2, otaa004. https://doi.org/10.1093/crocol/otaa004

Gampierakis, I.-A., Koutmani, Y., Semitekolou, M., Morianos, I., Polissidis, A., Katsouda, A., Charalampopoulos, I., Xanthou, G., Gravanis, A., Karalis, K.P., 2021. Hippocampal

neural stem cells and microglia response to experimental inflammatory bowel disease (IBD). Mol Psychiatry 26, 1248–1263. https://doi.org/10.1038/s41380-020-0651-6

Gloor, G., Fern, A., es, Macklaim, J., Albert, A., Links, M., Quinn, T., Wu, J.R., Wong, R.G., Br, Lieng, on, 2023. ALDEx2: Analysis Of Differential Abundance Taking Sample Variation Into Account. https://doi.org/10.18129/B9.bioc.ALDEx2

Gu, Z., Eils, R., Schlesner, M., 2016. Complex heatmaps reveal patterns and correlations in multidimensional genomic data. Bioinformatics 32, 2847–2849. https://doi.org/10.1093/bioinformatics/btw313

Günther, C., Rothhammer, V., Karow, M., Neurath, M., Winner, B., 2021. The Gut-Brain Axis in Inflammatory Bowel Disease—Current and Future Perspectives. Int J Mol Sci 22, 8870. https://doi.org/10.3390/ijms22168870

Gupta, N., Lustig, R.H., Andrews, H., Sylvester, F., Keljo, D., Goyal, A., Gokhale, R., Patel, A.S., Guthery, S., Leu, C.-S., 2020. Introduction to and Screening Visit Results of the Multicenter Pediatric Crohn's Disease Growth Study. Inflammatory Bowel Diseases 26, 1945–1950. https://doi.org/10.1093/ibd/izaa023

Hadley, W., 2016. ggplot2: Elegant Graphics for Data Analysis. Springer-Verlag New York.

Hammami, M.B., Mahadevan, U., 2020. Men With Inflammatory Bowel Disease: Sexual Function, Fertility, Medication Safety, and Prostate Cancer. Am J Gastroenterol 115, 526–534. https://doi.org/10.14309/ajg.0000000000000515

Harms, R.L., Fritz, F.J., Tobisch, A., Goebel, R., Roebroeck, A., 2017. Robust and fast nonlinear optimization of diffusion MRI microstructure models. Neuroimage 155, 82–96. https://doi.org/10.1016/j.neuroimage.2017.04.064

He, S., Li, H., Yu, Z., Zhang, F., Liang, S., Liu, H., Chen, H., Lü, M., 2021. The Gut Microbiome and Sex Hormone-Related Diseases. Frontiers in Microbiology 12.

Herzer, M., Denson, L.A., Baldassano, R.N., Hommel, K.A., 2011. Patient and parent psychosocial factors associated with health-related quality of life in pediatric inflammatory bowel disease. Journal of Pediatric Gastroenterology and Nutrition 52, 295–299. https://doi.org/10.1097/MPG.0b013e3181f5714e

Hildebrand, H., Karlberg, J., Kristiansson, B., 1994. Longitudinal growth in children and adolescents with inflammatory bowel disease. J Pediatr Gastroenterol Nutr 18, 165–173. https://doi.org/10.1097/00005176-199402000-00008

Hou, J., Dodd, K., Nair, V.A., Rajan, S., Beniwal-Patel, P., Saha, S., Prabhakaran, V., 2020. Alterations in brain white matter microstructural properties in patients with Crohn's disease in remission. Scientific Reports. https://doi.org/10.1038/s41598-020-59098-w

Jiang, Y., Johnson, G.A., 2011. Microscopic diffusion tensor atlas of the mouse brain. NeuroImage 56, 1235–1243. https://doi.org/10.1016/j.neuroimage.2011.03.031

Kaplan, G.G., Windsor, J.W., 2021. The four epidemiological stages in the global evolution of inflammatory bowel disease. Nat Rev Gastroenterol Hepatol 18, 56–66. https://doi.org/10.1038/s41575-020-00360-x

Kassambara, A., 2023. ggpubr: "ggplot2" Based Publication Ready Plots [WWW Document]. URL https://rpkgs.datanovia.com/ggpubr/

Katoh, K., Misawa, K., Kuma, K., Miyata, T., 2002. MAFFT: a novel method for rapid multiple sequence alignment based on fast Fourier transform. Nucleic Acids Research 30, 3059–3066. https://doi.org/10.1093/nar/gkf436

Keller, M., Baum, M.J., Bakker, J., 2008. Olfactory Control of Sex-Recognition and Sexual Behavior in Mice, in: Hurst, J.L., Beynon, R.J., Roberts, S.C., Wyatt, T.D. (Eds.), Chemical Signals in Vertebrates 11. Springer, New York, NY, pp. 241–250. https://doi.org/10.1007/978-0-387-73945-8_23

Kight, K.E., McCarthy, M.M., 2020. Androgens and the developing hippocampus. Biol Sex Differ 11, 30. https://doi.org/10.1186/s13293-020-00307-6

Kim, Jennifer, Pavlidis, Paul, Ciernia, Annie Vogel, A.V., 2023. Development of a high-throughput pipeline to characterize microglia morphological states at a single-cell resolution. bioRxiv. https://doi.org/10.1101/2023.11.03.565581

Klaus, J., Reinshagen, M., Adler, G., Boehm, B., von Tirpitz, C., 2008. Bones and Crohn's: Estradiol deficiency in men with Crohn's disease is not associated with reduced bone mineral density. BMC Gastroenterol 8, 48. https://doi.org/10.1186/1471-230X-8-48

Kleine Bardenhorst, S., Vital, M., Karch, A., Rübsamen, N., 2022. Richness estimation in microbiome data obtained from denoising pipelines. Computational and Structural Biotechnology Journal 20, 508–520. https://doi.org/10.1016/j.csbj.2021.12.036

Korpela, K., Kallio, S., Salonen, A., Hero, M., Kukkonen, A.K., Miettinen, P.J., Savilahti, E., Kohva, E., Kariola, L., Suutela, M., Tarkkanen, A., de Vos, W.M., Raivio, T., Kuitunen, M., 2021. Gut microbiota develop towards an adult profile in a sex-specific manner during puberty. Sci Rep 11, 23297. https://doi.org/10.1038/s41598-021-02375-z

Lavelle, A., Sokol, H., 2020. Gut microbiota-derived metabolites as key actors in inflammatory bowel disease. Nature Reviews Gastroenterology and Hepatology 17, 223–237. https://doi.org/10.1038/s41575-019-0258-z

Li, D., Liu, R., Wang, M., Peng, R., Fu, S., Fu, A., Le, J., Yao, Q., Yuan, T., Chi, H., Mu, X., Sun, T., Liu, H., Yan, P., Wang, S., Cheng, S., Deng, Z., Liu, Z., Wang, G., Li, Y., Liu, T., 2022. 3β-Hydroxysteroid dehydrogenase expressed by gut microbes degrades testosterone and is linked to depression in males. Cell Host & Microbe 30, 329-339.e5. https://doi.org/10.1016/j.chom.2022.01.001

Lv, K., Fan, Y.H., Xu, L., Xu, M.S., 2017. Brain changes detected by functional magnetic resonance imaging and spectroscopy in patients with Crohn's disease. World Journal of Gastroenterology. https://doi.org/10.3748/wjg.v23.i20.3607

Machiels, K., Joossens, M., Sabino, J., De Preter, V., Arijs, I., Eeckhaut, V., Ballet, V., Claes, K., Van Immerseel, F., Verbeke, K., Ferrante, M., Verhaegen, J., Rutgeerts, P., Vermeire, S., 2014. A decrease of the butyrate-producing species Roseburia hominis and Faecalibacterium prausnitzii defines dysbiosis in patients with ulcerative colitis. Gut 63, 1275–1283. https://doi.org/10.1136/gutjnl-2013-304833

Mackner, L.M., Greenley, R.N., Szigethy, E., Herzer, M., Deer, K., Hommel, K.A., 2013. Psychosocial Issues in Pediatric Inflammatory Bowel Disease: A Clinical Report of the North American Society for Pediatric Gastroenterology, Hepatology and Nutrition. J Pediatr Gastroenterol Nutr 56, 449–458. https://doi.org/10.1097/MPG.0b013e3182841263

Maffei, S., Forini, F., Canale, P., Nicolini, G., Guiducci, L., 2022. Gut Microbiota and Sex Hormones: Crosstalking Players in Cardiometabolic and Cardiovascular Disease. International Journal of Molecular Sciences 23, 7154. https://doi.org/10.3390/ijms23137154

Malkesman, O., Scattoni, M.L., Paredes, D., Tragon, T., Pearson, B., Shaltiel, G., Chen, G., Crawley, J.N., Manji, H.K., 2010. The Female Urine Sniffing Test: A Novel Approach for Assessing Reward-Seeking Behavior in Rodents. Biol Psychiatry 67, 864–871. https://doi.org/10.1016/j.biopsych.2009.10.018

Mandal, S., Van Treuren, W., White, R.A., Eggesbø, M., Knight, R., Peddada, S.D., 2015. Analysis of composition of microbiomes: a novel method for studying microbial composition. Microb Ecol Health Dis 26, 27663. https://doi.org/10.3402/mehd.v26.27663

Markle, J.G.M., Frank, D.N., Mortin-Toth, S., Robertson, C.E., Feazel, L.M., Rolle-Kampczyk, U., von Bergen, M., McCoy, K.D., Macpherson, A.J., Danska, J.S., 2013. Sex Differences in the Gut Microbiome Drive Hormone-Dependent Regulation of Autoimmunity. Science 339, 1084–1088. https://doi.org/10.1126/science.1233521

McMurdie, P.J., Holmes, S., 2013. phyloseq: An R Package for Reproducible Interactive Analysis and Graphics of Microbiome Census Data. PLOS ONE 8, e61217. https://doi.org/10.1371/journal.pone.0061217

Mertens, K.L., Kalsbeek, A., Soeters, M.R., Eggink, H.M., 2017. Bile Acid Signaling Pathways from the Enterohepatic Circulation to the Central Nervous System. Frontiers in Neuroscience 11.

Min, S.H., Zhou, J., 2021. smplot: An R Package for Easy and Elegant Data Visualization. Front. Genet. 12. https://doi.org/10.3389/fgene.2021.802894

Mirzaei, R., Bouzari, B., Hosseini-Fard, S.R., Mazaheri, M., Ahmadyousefi, Y., Abdi, M., Jalalifar, S., Karimitabar, Z., Teimoori, A., Keyvani, H., Zamani, F., Yousefimashouf, R., Karampoor, S., 2021. Role of microbiota-derived short-chain fatty acids in nervous

system disorders. Biomed Pharmacother 139, 111661. https://doi.org/10.1016/j.biopha.2021.111661

Mitchell, R.W., On, N.H., Del Bigio, M.R., Miller, D.W., Hatch, G.M., 2011. Fatty acid transport protein expression in human brain and potential role in fatty acid transport across human brain microvessel endothelial cells. J Neurochem 117, 735–746. https://doi.org/10.1111/j.1471-4159.2011.07245.x

Munyaka, P.M., Rabbi, M.F., Khafipour, E., Ghia, J., 2016. Acute dextran sulfate sodium (DSS)-induced colitis promotes gut microbial dysbiosis in mice. J. Basic Microbiol. 56, 986–998. https://doi.org/10.1002/jobm.201500726

Naser, S.A., Sagramsingh, S.R., Naser, A.S., Thanigachalam, S., 2014. Mycobacterium avium subspecies paratuberculosis causes Crohn's disease in some inflammatory bowel disease patients. World J Gastroenterol 20, 7403–7415. https://doi.org/10.3748/wjg.v20.i23.7403

Nasser, M., Haider, A., Saad, F., Kurtz, W., Doros, G., Fijak, M., Vignozzi, L., Gooren, L., 2015. Testosterone therapy in men with Crohn's disease improves the clinical course of the disease: data from long-term observational registry study. Horm Mol Biol Clin Investig 22, 111–117. https://doi.org/10.1515/hmbci-2015-0014

Neuman, H., Debelius, J.W., Knight, R., Koren, O., 2015. Microbial endocrinology: the interplay between the microbiota and the endocrine system. FEMS Microbiology Reviews 39, 509–521. https://doi.org/10.1093/femsre/fuu010

Ng, K.M., Pannu, S., Liu, S., Burckhardt, J.C., Hughes, T., Van Treuren, W., Nguyen, J., Naqvi, K., Nguyen, B., Clayton, C.A., Pepin, D.M., Collins, S.R., Tropini, C., 2023. Single-strain behavior predicts responses to environmental pH and osmolality in the gut microbiota. mBio 14, e00753-23. https://doi.org/10.1128/mbio.00753-23

Ng, K.M., Tropini, C., 2021. Visualization of Gut Microbiota-host Interactions via Fluorescence In Situ Hybridization, Lectin Staining, and Imaging. JoVE (Journal of Visualized Experiments) e62646. https://doi.org/10.3791/62646

Ng, S.C., Shi, H.Y., Hamidi, N., Underwood, F.E., Tang, W., Benchimol, E.I., Panaccione, R., Ghosh, S., Wu, J.C.Y., Chan, F.K.L., Sung, J.J.Y., Kaplan, G.G., 2017. Worldwide incidence and prevalence of inflammatory bowel disease in the 21st century: a systematic review of population-based studies. The Lancet. https://doi.org/10.1016/S0140-6736(17)32448-0

Nyuyki, K.D., Cluny, N.L., Swain, M.G., Sharkey, K.A., Pittman, Q.J., 2018. Altered brain excitability and increased anxiety in mice with experimental colitis: Consideration of hyperalgesia and sex differences. Frontiers in Behavioral Neuroscience 12, 1–11. https://doi.org/10.3389/fnbeh.2018.00058

Okayasu, I., Hatakeyama, S., Yamada, M., Ohkusa, T., Inagaki, Y., Nakaya, R., 1990. A novel method in the induction of reliable experimental acute and chronic ulcerative colitis in mice. Gastroenterology 98, 694–702. https://doi.org/10.1016/0016-5085(90)90290-h

Patel, J., Chaudhary, H., Rajput, K., Parekh, B., Joshi, R., 2023. Assessment of gut microbial β-glucuronidase and β-glucosidase activity in women with polycystic ovary syndrome. Sci Rep 13, 11967. https://doi.org/10.1038/s41598-023-39168-5

Price, M.N., Dehal, P.S., Arkin, A.P., 2010. FastTree 2 – Approximately Maximum-Likelihood Trees for Large Alignments. PLOS ONE 5, e9490. https://doi.org/10.1371/journal.pone.0009490

Quast, C., Pruesse, E., Yilmaz, P., Gerken, J., Schweer, T., Yarza, P., Peplies, J., Glöckner, F.O., 2013. The SILVA ribosomal RNA gene database project: improved data processing and web-based tools. Nucleic Acids Res 41, D590–D596. https://doi.org/10.1093/nar/gks1219

R Core team, 2021. R: A language and environment for statistical computing [WWW Document]. URL https://www.r-project.org/ (accessed 4.1.23).

Roda, G., Chien Ng, S., Kotze, P.G., Argollo, M., Panaccione, R., Spinelli, A., Kaser, A., Peyrin-Biroulet, L., Danese, S., 2020. Crohn's disease. Nat Rev Dis Primers 6, 1–19. https://doi.org/10.1038/s41572-020-0156-2

Rosen, M.J., Dhawan, A., Saeed, S.A., 2015. Inflammatory Bowel Disease in Children and Adolescents. JAMA Pediatr 169, 1053–1060. https://doi.org/10.1001/jamapediatrics.2015.1982

Ruemmele, F.M., Turner, D., 2014. Differences in the management of pediatric and adult onset ulcerative colitis — lessons from the joint ECCO and ESPGHAN consensus guidelines for the management of pediatric ulcerative colitis. Journal of Crohn's and Colitis 8, 1–4. https://doi.org/10.1016/j.crohns.2013.10.006

Salvo, E., Stokes, P., Keogh, C.E., Brust-Mascher, I., Hennessey, C., Knotts, T.A., Sladek, J.A., Rude, K.M., Swedek, M., Rabasa, G., Gareau, M.G., 2020. A murine model of pediatric inflammatory bowel disease causes microbiota-gut-brain axis deficits in adulthood. Am J Physiol Gastrointest Liver Physiol 319, G361–G374. https://doi.org/10.1152/ajpgi.00177.2020

Silva, Y.P., Bernardi, A., Frozza, R.L., 2020. The Role of Short-Chain Fatty Acids From Gut Microbiota in Gut-Brain Communication. Frontiers in Endocrinology 11. https://doi.org/10.3389/fendo.2020.00025

Sinha, S.R., Haileselassie, Y., Nguyen, L.P., Tropini, C., Wang, M., Becker, L.S., Sim, D., Jarr, K., Spear, E.T., Singh, G., Namkoong, H., Bittinger, K., Fischbach, M.A., Sonnenburg, J.L., Habtezion, A., 2020. Dysbiosis-Induced Secondary Bile Acid Deficiency Promotes Intestinal Inflammation. Cell Host Microbe 27, 659-670.e5. https://doi.org/10.1016/j.chom.2020.01.021

Smith, S.M., Jenkinson, M., Woolrich, M.W., Beckmann, C.F., Behrens, T.E.J., Johansen-Berg, H., Bannister, P.R., De Luca, M., Drobnjak, I., Flitney, D.E., Niazy, R.K., Saunders, J., Vickers, J., Zhang, Y., De Stefano, N., Brady, J.M., Matthews, P.M., 2004. Advances in functional and structural MR image analysis and implementation as FSL. Neuroimage 23 Suppl 1, S208-219. https://doi.org/10.1016/j.neuroimage.2004.07.051

Sokol, H., Pigneur, B., Watterlot, L., Lakhdari, O., Bermúdez-Humarán, L.G., Gratadoux, J.J., Blugeon, S., Bridonneau, C., Furet, J.P., Corthier, G., Grangette, C., Vasquez, N., Pochart, P., Trugnan, G., Thomas, G., Blottière, H.M., Doré, J., Marteau, P., Seksik, P., Langella, P., 2008. Faecalibacterium prausnitzii is an anti-inflammatory commensal bacterium identified by gut microbiota analysis of Crohn disease patients. Proceedings of the National Academy of Sciences of the United States of America 105, 16731–16736. https://doi.org/10.1073/pnas.0804812105

Sroor, H.M., Hassan, A.M., Zenz, G., Valadez-Cosmes, P., Farzi, A., Holzer, P., El-Sharif, A., Gomaa, F.A.-Z.M., Kargl, J., Reichmann, F., 2019. Experimental colitis reduces microglial cell activation in the mouse brain without affecting microglial cell numbers. Sci Rep 9, 20217. https://doi.org/10.1038/s41598-019-56859-0

Stahl, M., Graef, F.A., Vallance, B.A., 2017. Mouse Models for Campylobacter jejuni Colonization and Infection, in: Butcher, J., Stintzi, A. (Eds.), Campylobacter Jejuni:

Methods and Protocols. Springer, New York, NY, pp. 171–188. https://doi.org/10.1007/978-1-4939-6536-6_15

Sui, Y., Wu, J., Chen, J., 2021. The Role of Gut Microbial β-Glucuronidase in Estrogen Reactivation and Breast Cancer. Front Cell Dev Biol 9, 631552. https://doi.org/10.3389/fcell.2021.631552

Sullivan, O., Ciernia, A.V., 2022. Work hard, play hard: how sexually differentiated microglia work to shape social play and reproductive behavior. Frontiers in Behavioral Neuroscience 16.

Talley, S., Valiauga, R., Anderson, L., Cannon, A.R., Choudhry, M.A., Campbell, E.M., 2021. DSS-induced inflammation in the colon drives a proinflammatory signature in the brain that is ameliorated by prophylactic treatment with the S100A9 inhibitor paquinimod. Journal of Neuroinflammation 18, 263. https://doi.org/10.1186/s12974-021-02317-6

Terstege, D.J., Oboh, D.O., Epp, J.R., 2022. FASTMAP: Open-Source Flexible Atlas Segmentation Tool for Multi-Area Processing of Biological Images. eNeuro 9, ENEURO.0325-21.2022. https://doi.org/10.1523/ENEURO.0325-21.2022

Thavamani, A., Umapathi, K.K., Khatana, J., Gulati, R., 2019. Burden of Psychiatric Disorders among Pediatric and Young Adults with Inflammatory Bowel Disease: A Population-Based Analysis. Pediatr Gastroenterol Hepatol Nutr 22, 527–535. https://doi.org/10.5223/pghn.2019.22.6.527

Thibault, R., Blachier, F., Darcy-Vrillon, B., de Coppet, P., Bourreille, A., Segain, J.-P., 2010. Butyrate utilization by the colonic mucosa in inflammatory bowel diseases: a transport deficiency. Inflamm Bowel Dis 16, 684–695. https://doi.org/10.1002/ibd.21108

Thion, M.S., Low, D., Silvin, A., Chen, J., Grisel, P., Schulte-Schrepping, J., Blecher, R., Ulas, T., Squarzoni, P., Hoeffel, G., Coulpier, F., Siopi, E., David, F.S., Scholz, C., Shihui, F., Lum, J., Amoyo, A.A., Larbi, A., Poidinger, M., Buttgereit, A., Lledo, P.-M., Greter, M., Chan, J.K.Y., Amit, I., Beyer, M., Schultze, J.L., Schlitzer, A., Pettersson, S., Ginhoux, F., Garel, S., 2017. Microbiome Influences Prenatal and Adult Microglia in a Sex-Specific Manner. Cell 1–17. https://doi.org/10.1016/j.cell.2017.11.042

Tigas, S., Tsatsoulis, A., 2012. Endocrine and metabolic manifestations in inflammatory bowel disease. Ann Gastroenterol 25, 37–44.

Torres, J., Mehandru, S., Colombel, J.-F., Peyrin-Biroulet, L., 2017. Crohn's disease. Lancet 389, 1741–1755. https://doi.org/10.1016/S0140-6736(16)31711-1

Torres, P.J., Siakowska, M., Banaszewska, B., Pawelczyk, L., Duleba, A.J., Kelley, S.T., Thackray, V.G., 2018. Gut Microbial Diversity in Women With Polycystic Ovary Syndrome Correlates With Hyperandrogenism. J Clin Endocrinol Metab 103, 1502–1511. https://doi.org/10.1210/jc.2017-02153

van Griethuysen, J.J.M., Fedorov, A., Parmar, C., Hosny, A., Aucoin, N., Narayan, V., Beets-Tan, R.G.H., Fillion-Robin, J.-C., Pieper, S., Aerts, H.J.W.L., 2017. Computational Radiomics System to Decode the Radiographic Phenotype. Cancer Res 77, e104–e107. https://doi.org/10.1158/0008-5472.CAN-17-0339

Vogel Ciernia, A., Careaga, M., LaSalle, J.M., Ashwood, P., 2018. Microglia from offspring of dams with allergic asthma exhibit epigenomic alterations in genes dysregulated in autism. Glia 66, 505–521. https://doi.org/10.1002/glia.23261

Vogel-Ciernia, A., Wood, M.A., 2014. Examining object location and object recognition memory in mice. Current Protocols in Neuroscience 2014, 8.31.1-8.31.17. https://doi.org/10.1002/0471142301.ns0831s69

Weger, B.D., Gobet, C., Yeung, J., Martin, E., Jimenez, S., Betrisey, B., Foata, F., Berger, B., Balvay, A., Foussier, A., Charpagne, A., Boizet-Bonhoure, B., Chou, C.J., Naef, F., Gachon, F., 2019. The Mouse Microbiome Is Required for Sex-Specific Diurnal Rhythms of Gene Expression and Metabolism. Cell Metab 29, 362-382.e8. https://doi.org/10.1016/j.cmet.2018.09.023

Wenzel, T.J., Gates, E.J., Ranger, A.L., Klegeris, A., 2020. Short-chain fatty acids (SCFAs) alone or in combination regulate select immune functions of microglia-like cells. Molecular and Cellular Neuroscience 105, 103493. https://doi.org/10.1016/j.mcn.2020.103493

Wickham, H., Averick, M., Bryan, J., Chang, W., McGowan, L.D., François, R., Grolemund, G., Hayes, A., Henry, L., Hester, J., Kuhn, M., Pedersen, T.L., Miller, E., Bache, S.M., Müller, K., Ooms, J., Robinson, D., Seidel, D.P., Spinu, V., Takahashi, K., Vaughan, D., Wilke, C., Woo, K., Yutani, H., 2019. Welcome to the Tidyverse. Journal of Open Source Software 4, 1686. https://doi.org/10.21105/joss.01686

Wirtz, S., Neurath, M.F., 2007. Mouse models of inflammatory bowel disease. Advanced Drug Delivery Reviews, Prediction of Therapeutic and Drug Delivery Outcomes Using Animal Models 59, 1073–1083. https://doi.org/10.1016/j.addr.2007.07.003

Yamane, T., Kitamura, Y., Terada, N., Matsumoto, K., 1986. Proliferative response of seminal vesicle cells to androgen and estrogen in neonatally castrated mice. Journal of Steroid Biochemistry 24, 703–708. https://doi.org/10.1016/0022-4731(86)90846-0

Yang, M., Crawley, J.N., 2009. Simple behavioral assessment of mouse olfaction. Curr Protoc Neurosci Chapter 8, Unit 8.24. https://doi.org/10.1002/0471142301.ns0824s48

Ye, Y., Pang, Z., Chen, W., Ju, S., Zhou, C., 2015. The epidemiology and risk factors of inflammatory bowel disease. Int J Clin Exp Med 8, 22529–22542.

Yi, S.Y., Barnett, B.R., Torres-Velázquez, M., Zhang, Y., Hurley, S.A., Rowley, P.A., Hernando, D., Yu, J.-P.J., 2019. Detecting Microglial Density With Quantitative Multi-Compartment Diffusion MRI. Front Neurosci 13, 81. https://doi.org/10.3389/fnins.2019.00081

Zhang, H., Schneider, T., Wheeler-Kingshott, C.A., Alexander, D.C., 2012. NODDI: practical in vivo neurite orientation dispersion and density imaging of the human brain. Neuroimage 61, 1000–1016. https://doi.org/10.1016/j.neuroimage.2012.03.072

Zhang, J., Wei, S., Zeng, Q., Wu, X., Gan, H., 2021. Prevalence and risk factors of sexual dysfunction in patients with inflammatory bowel disease: systematic review and meta-analysis. Int J Colorectal Dis 36, 2027–2038. https://doi.org/10.1007/s00384-021-03958-y

Zhao, S., Wang, J., Liu, Y., Luo, L., Zhu, Z., Li, E., Luo, J., Zhao, Z., 2019. Inflammatory Bowel Diseases Were Associated With Risk of Sexual Dysfunction in Both Sexes: A Meta-analysis. Inflamm Bowel Dis 25, 699–707. https://doi.org/10.1093/ibd/izy345

Zhou, Y., Ji, G., Yang, X., Chen, Z., Zhou, L., 2023. Behavioral abnormalities in C57BL/6 mice with chronic ulcerative colitis induced by DSS. BMC Gastroenterology 23, 84. https://doi.org/10.1186/s12876-023-02718-2

Ziętek, M., Celewicz, Z., Szczuko, M., 2021. Short-Chain Fatty Acids, Maternal Microbiota and Metabolism in Pregnancy. Nutrients 13, 1244. https://doi.org/10.3390/nu13041244